This is a repository copy of *Toll-like receptor 3 is a therapeutic target for pulmonary hypertension*.

White Rose Research Online URL for this paper:
http://eprints.whiterose.ac.uk/135777/

Version: Accepted Version

Article:
Farkas, D., Thompson, A.A.R. orcid.org/0000-0002-0717-4551, Bhagwani, A.R. et al. (14 more authors) (2018) Toll-like receptor 3 is a therapeutic target for pulmonary hypertension. American Journal of Respiratory and Critical Care Medicine. ISSN 1073-449X

https://doi.org/10.1164/rccm.201707-1370OC

Originally Published in: Farkas et al. Toll-like Receptor 3 is a Therapeutic Target for Pulmonary Hypertension. American Journal of Respiratory and Critical Care Medicine 2018. DOI: 10.1164/rccm.201707-1370OC Copyright © 2018 by the American Thoracic Society The final publication is available at:
https://www.atsjournals.org/doi/10.1164/rccm.201707-1370OC

Reuse
Items deposited in White Rose Research Online are protected by copyright, with all rights reserved unless indicated otherwise. They may be downloaded and/or printed for private study, or other acts as permitted by national copyright laws. The publisher or other rights holders may allow further reproduction and re-use of the full text version. This is indicated by the licence information on the White Rose Research Online record for the item.

Takedown
If you consider content in White Rose Research Online to be in breach of UK law, please notify us by emailing eprints@whiterose.ac.uk including the URL of the record and the reason for the withdrawal request.

eprints@whiterose.ac.uk
https://eprints.whiterose.ac.uk/

AJRCCM Articles in Press. Published on 13-September-2018 as 10.1164/rccm.201707-1370OC

Toll-like receptor 3 is a therapeutic target for Pulmonary Hypertension

Daniela Farkas [1]*, A. A. Roger Thompson [2]*, Aneel R. Bhagwani [1], Schuyler Hultman [1], Hyun Ji [1], Naveen Kotha [1], Grant Farr [1], Nadine D. Arnold [2], Adam Braithwaite [2], Helen Casbolt [2], Jennifer E. Cole [3], Ian Sabroe [2], Claudia Monaco [3], Carlyne D. Cool [4], Elena A. Goncharova [5], Allan Lawrie [2], Laszlo Farkas [1]

* These authors contributed equally

Affiliations:
[1] Division of Pulmonary Disease and Critical Care Medicine, Department of Internal Medicine, Virginia Commonwealth University, Richmond, VA, USA
[2] Department of Infection, Immunity & Cardiovascular Disease, Faculty of Medicine, Dentistry & Health, University of Sheffield, Sheffield, UK
[3] Kennedy Institute of Rheumatology, University of Oxford, Oxford, UK
[4] Department of Pathology, University of Colorado Denver, Denver, CO, USA
[5] Pittsburgh Heart, Lung and Blood Vascular Medicine Institute, Division of Pulmonary, Allergy, and Critical Care Medicine, Department of Medicine, Department of Bioengineering, University of Pittsburgh, Pittsburgh, PA

Short title: Pulmonary Hypertension and Toll-like receptor 3

Corresponding author: Laszlo Farkas, M.D.
Division of Pulmonary Disease and Critical Care Medicine,
Department of Internal Medicine
Virginia Commonwealth University
MCV Campus, Molecular Medicine Research Building
1220 E Broad Street,
P.O. Box 980456
Richmond, VA, 23298, USA
Email: laszlo.farkas@vcuhealth.org; lfarkasmd@gmail.com

Author contributions: Conception & Design (DF, AART, ARB, SH, GF, NDA, AB, HC, JEC, IS, CM, CDC, EAG, AL, LF), Data acquisition & analysis (DF, AART, ARB, SH, HJ, NK, GF, NDA, AB, HC, IS, AL, LF), Article drafting/revision (DF, AART, ARB, SH, GF, NDA, AB, JC, JEC, IS, CM, CDC, EAG, AL, LF), Final approval (all authors).

Sources of Support: AART was supported by a NIHR Clinical Lectureship and a British Heart Foundation-Fulbright Scholarship award. ARB was supported by a Fulbright Scholarship award. AL was supported by a British Heart Foundation Senior Basic Science Research Fellowship (FS/13/48/30453). The work was further supported by grants from the American Heart Association (13SDG16360018) and NIH/NHLBI (HL114816, HL123044) to LF. University of Pittsburgh Cell Processing core was supported by P01 HL103455 to EAG. Confocal microscopy was performed at the VCU Microscopy Facility, supported, in part, by funding from NIH-NCI Cancer Center Support

Copyright © 2018 by the American Thoracic Society

Grant P30 CA016059. Services and products in support of the research project were generated by the VCU Massey Cancer Center Flow Cytometry Shared Resource, supported, in part, with funding from NIH-NCI Cancer Center Support Grant P30 CA016059. Data/Tissue samples provided by PHBI under the Pulmonary Hypertension Breakthrough Initiative (PHBI). Funding for the PHBI is provided under an NHLBI R24 grant, R24HL123767, and by the Cardiovascular Medical Research and Education Fund (CMREF).

Descriptor number: 17.6 Pulmonary Hypertension: Experimental

Total word count: 3,365

At a Glance Commentary:

Scientific Knowledge on the Subject

Endothelial cell apoptosis contributes to the vascular remodeling in Pulmonary Hypertension. But the pathways causing endothelial cell apoptosis are only partially understood. Current concepts indicate a role for chronic inflammation in Pulmonary Hypertension, yet innate RNA recognition may also be a protective mechanism in the vasculature.

What This Study Adds to the Field

Here we demonstrate, for the first time, that Toll-like receptor 3 (TLR3) expression is reduced in lung tissue and endothelial cells from patients with Pulmonary Hypertension and show *in vitro* and *in vivo* that TLR3 deficiency increases susceptibility to apoptosis and Pulmonary Hypertension. We further show that the TLR3 agonist and double stranded RNA Polyinosinic:polycytidylic acid increases TLR3 expression and reduces established Pulmonary Hypertension. Our data suggest that this protective upregulation of TLR3 involves induction of interleukin 10. We propose that TLR3 expression is required for endothelial cell homeostasis and that restoring TLR3 signaling may be a

Copyright © 2018 by the American Thoracic Society

AJRCCM Articles in Press. Published on 13-September-2018 as 10.1164/rccm.201707-1370OC

novel avenue to complement existing treatment strategies in Pulmonary Hypertension.

Subject codes: Pulmonary Hypertension, Inflammation, Endothelium, Vascular Biology, Gene expression

Link to publisher's version: https://www.atsjournals.org/doi/abs/10.1164/rccm.201707-1370OC

Copyright © 2018 by the American Thoracic Society

ABSTRACT

Rationale: Pulmonary arterial hypertension (PAH) is characterized by vascular cell proliferation and endothelial cell apoptosis. Toll-like receptor 3 (TLR3) is a receptor for double-stranded RNA and has been recently implicated in vascular protection.

Objective: The goal was to study the expression and role of TLR3 in PAH and to determine whether a TLR3 agonist reduces Pulmonary Hypertension in preclinical models.

Methods: Lung tissue and endothelial cells from PAH patients were investigated by polymerase chain reaction, immunofluorescence and apoptosis assays. $TLR3^{-/-}$ and $TLR3^{+/+}$ mice were exposed to chronic hypoxia and SU5416. Chronic hypoxia or chronic hypoxia/SU5416 rats were treated with the TLR3 agonist polyinosinic:polycytidylic acid [Poly(I:C)].

Measurements and Main Results: TLR3 expression was reduced in PAH patient lung tissue and endothelial cells, and $TLR3^{-/-}$ mice exhibited more severe Pulmonary Hypertension following exposure to chronic hypoxia/SU5416. TLR3 knockdown promoted double-stranded RNA signaling *via* other intracellular RNA receptors in endothelial cells and this was associated with greater susceptibility to apoptosis, a known driver of pulmonary vascular remodeling. Poly(I:C) increased TLR3 expression via interleukin-10 in rat endothelial cells. *In vivo*, high dose Poly(I:C) reduced Pulmonary Hypertension in both rat models in proof-of-principle experiments. In addition, Poly(I:C) also reduced right ventricular failure in established Pulmonary Hypertension.

Conclusions: Our work identifies a novel role for TLR3 in PAH based on the findings that reduced expression of TLR3 contributes to endothelial apoptosis and pulmonary vascular remodeling.

Copyright © 2018 by the American Thoracic Society

AJRCCM Articles in Press. Published on 13-September-2018 as 10.1164/rccm.201707-1370OC

Abstract word count: 229

Key words: Pulmonary Hypertension, toll-like receptor 3, endothelial cell, double stranded RNA, apoptosis

Copyright © 2018 by the American Thoracic Society

INTRODUCTION

Pulmonary arterial hypertension (PAH) is a severe and progressive disease of the pulmonary arterial bed and is characterized by occlusive remodeling of pulmonary arteries (1). While current therapies improve quality of life and prognosis, PAH remains a life-limiting condition (2). One reason is that the current treatment options do little to change the chronic pathology in the pulmonary arteries (3). Apoptosis of endothelial cells (EC) contributes to lung vascular remodeling by promoting selection of apoptosis-resistant EC, initiating proliferation of vascular smooth muscle cells (VSMC), and directly, *via* vascular pruning (4–11). Multiple pathogenic mechanisms likely contribute to EC apoptosis (7–10) and identifying targetable mechanisms remains an important goal (11).

Recently, a protective role in blood vessels was shown for Toll-like receptor 3 (TLR3), a member of the TLR family of innate immune receptors (12). TLR3 responds to viral and synthetic double-stranded (ds) RNA, as well as RNA released from healthy and apoptotic cells (13; 14). TLR3 not only regulates RNA signaling by its primary localization at the endosomal membrane, but TLR3 can also influence RNA signaling through additional cytosolic RNA receptors. These RNA receptors include Retinoic Acid-inducible Gene-I (RIG-I) and Melanoma Differentiation-Associated Protein-5 (MDA-5) (15; 16).

In addition to the role of TLR3 in the intracellular response to RNA, a protective effect has been shown for the synthetic dsRNA and TLR3 agonist polyinosinic:polycytidylic acid [Poly(I:C)]. This protection was in part mediated via the anti-inflammatory cytokine interleukin-10 (IL-10) (12; 17)

Based on this evidence, we hypothesized that TLR3 signaling protects lung vasculature, and that promoting TLR3 signaling would reduce PH. We therefore

Copyright © 2018 by the American Thoracic Society

AJRCCM Articles in Press. Published on 13-September-2018 as 10.1164/rccm.201707-1370OC

examined TLR3 expression and show that endothelial expression of TLR3 is reduced in occlusive vascular lesions, pulmonary artery EC (PAEC) and lung tissue from patients with PAH. TLR3 knockout exaggerated PH and endothelial apoptosis in mice exposed to chronic hypoxia and SU5416 (cHx/Su). *In vitro*, exposure to high, but not low, concentrations of dsRNA promoted TLR3 expression by increasing IL-10 expression in $CD117^+$ lung EC. *In vivo*, treatment with high dose Poly(I:C) prevented and reduced experimental PH in rats in proof-of-principle experiments, ameliorating vascular remodeling, apoptosis and proliferation in pulmonary arteries. Some of the results of these studies have been previously reported in the form of abstracts (18–20).

METHODS

Human tissue samples and endothelial cells

De-identified human lung tissue was obtained from the Department of Pathology, University of Colorado Denver and the tissue repository of the Pulmonary Hypertension Breakthrough Initiative (PHBI). PAEC were isolated by the University of Pittsburgh Cell Processing Core and the PHBI in a de-identified manner under PHBI-approved protocols and in compliance with the Institutional Review Boards. Control samples and cells were from failed donor lungs and lung tissue resections for other diseases, e.g., cancer. The Institutional Review Boards have approved the tissue collection at the respective institutions. Due to the use of de-identified tissues and cells, the study was deemed non-human subjects research by the Office of Research Subjects Protection at Virginia Commonwealth University.

In vivo treatment in animal models

Copyright © 2018 by the American Thoracic Society

All animal experiments were approved by the Institutional Animal Care and Utilization Committees in accordance with the Health Research Extension Act (Public Law 99-158) at Virginia Commonwealth University and the U.K Home Office Animals (Scientific Procedures) Act of 1986 at the University of Sheffield. The procedures followed the "Guide for the Care and Use of Laboratory Animals", National Academy Press, Washington, D.C. 1996. Additional details regarding the experimental models and strains are found in an online data supplement. The treatment was applied as follows: Preventive strategy (cHx and cHx/Su): 1 mg/kg (only cHx/Su), 10 mg/kg Poly(I:C) or vehicle (PBS) three times a week by intraperitoneal (i.p.) injection from day 1-21; Therapeutic strategy (cHx/Su): 10 mg/kg Poly(I:C) three times a week i.p. from day 29-42. Additional controls were naive rats treated with 10 mg/kg Poly(I:C) or vehicle for 14 days. Animals were randomly assigned to the treatment groups. At day 21 or 42, the animals underwent echocardiographic and hemodynamic evaluation under anesthesia with Ketamine 100 mg/kg and Xylazine 15 mg/kg i.p., followed by tissue harvest after exsanguination (10; 21). In mice, right ventricular pressure-volume measurements were collected under isoflurane anesthesia as previously described (22).

Additional detail on the methods for cell culture experiments and animal experimentation is provided in an online data supplement.

Statistical Analysis

Data were compared using Student’s t-test (2 groups), or one or two-way ANOVA (more than 2 groups), following by multiple comparison testing using the Holm-Sidak or

Copyright © 2018 by the American Thoracic Society

AJRCCM Articles in Press. Published on 13-September-2018 as 10.1164/rccm.201707-1370OC

Sidak tests. The calculations were performed using Prism 6.0 (GraphPad Software Inc., San Diego, CA). A *P* value of <0.05 was considered significant.

RESULTS

Reduced TLR3 is associated with PAH and loss of TLR3 promotes severe PH *in vivo*.

Triple immunofluorescence (IF) showed reduced endothelial TLR3 staining in remodeled pulmonary arteries from PAH patients. In arteries with intima lesions, a part of the endothelium has lost TLR3 expression (Figure 1). Loss of TLR3 was widespread in the endothelium of concentric and plexiform lesions. In contrast, pulmonary artery endothelium of control subjects had strong TLR3 expression (Figure 1). We further confirmed reduced endothelial TLR3 expression in cultured PAEC and PAH lung tissue (Figure 2A-D). We further studied the timing of TLR3 expression in the cHx and cHx/Su PH models. TLR3 protein expression was lower in cHx/Su lung tissue at day 21 (Figure 2E-F), and cHx and cHx/Su animals had reduced fraction of $TLR3^{+}$ EC (Figure 2G-H).

Then, we evaluated TLR3 deficiency *in vivo*. Naive $TLR3^{-/-}$ mice failed to develop spontaneous PH (Figure 2I-L). However, media wall thickness (MWT), fraction of muscularized arteries and PH were aggravated in $TLR3^{-/-}$ mice following exposure to cHx/Su (Figure 2I-L). These data suggest that loss of TLR3 altered vascular function, leading to increased remodeling. Because of the importance of endothelial apoptosis in PAH pathobiology, we next sought to determine the link between TLR3 deficiency, endothelial apoptosis and PH.

TLR3 deficiency promotes endothelial apoptosis *in vivo*

Copyright © 2018 by the American Thoracic Society

Then we studied a potential driver of PH, apoptosis, in relation to TLR3 expression. While we found no apoptosis in TLR3-expressing endothelium from control subjects, we found TLR3-deficient apoptotic intima cells in PAH lesions (online supplement Figure E1A). Further analysis revealed an increased fraction of cleaved caspase-3^{+} intima cells in PAH pulmonary arteries (online supplement Figure E1B-C). Likewise, pulmonary arteries of TLR3$^{-/-}$ mice had more apoptotic EC after 21 days of cHx/Su (online supplement Figure E1D-E). We did not find increased apoptosis at early timepoints (1 or 6 days) in cHx/Su rats (online supplement Figure E2).

TLR3 deficiency promotes endothelial apoptosis *in vitro*

In vitro, PAH PAEC had elevated frequency of background apoptosis (Figure 3A-B) and we tested whether TLR3 deficiency promotes endothelial apoptosis using two approaches. First, we silenced TLR3 expression in rat lung CD117^{+} EC using single hairpin RNA (shRNA). These cells were isolated from the lungs of naive rats, expressed the endothelial marker vWF, formed angiogenic tubes and were clonally expandable (online supplement Figure E3). TLR3 knockdown increased the frequency of background apoptosis (Figure 3C-E). As second approach, we induced loss of TLR3 in human PAEC using Clustered Regularly Interspaced Short Palindromic Repeats (CRISPR)/Cas9 technology. We found in TLR3 CRISPR cells a substantial reduction in TLR3 protein (Figure 3F-H), which was maintained after passage (online supplement Figure E4). Because PAEC were in passage 5 or higher at the start of the experiment, we did not perform a selection of TLR3^{-} PAECs, retaining a small fraction of TLR3^{+} cells. TLR3 CRISPR PAEC had higher baseline expression of *DDX58* (RIG-I) and *IFIH1* (MDA-5) (Figure 3I), and a higher baseline apoptosis rate with an exaggerated apoptotic response

Copyright © 2018 by the American Thoracic Society

AJRCCM Articles in Press. Published on 13-September-2018 as 10.1164/rccm.201707-1370OC

to serum starvation (Figure 3J-K). TLR3 CRISPR also impaired migration *in vitro*. This was partially reversed by caspase inhibition, despite a small reduction in gap closure by the caspase inhibitor in scrm PAEC (Figure 3L-M).

Reduced TLR3 expression promotes RNA signaling via alternate RNA receptors RIG-I and MDA-5

We then evaluated the subcellular localization of dsRNA by exposing $CD117^+$ EC to rhodamine-labeled Poly(I:C) after treatment with scrambled shRNA (shscrm) or TLR3-targeted shRNA (shTLR3). In shTLR3 cells, Poly(I:C) localized to RIG-I and MDA-5 in the cytoplasm, whereas Poly(I:C) also localized to TLR3 in shscrm cells (Figure 4A). In shscrm EC, Poly(I:C) induced expression of *Cxcl10* and interleukin-6 (*Il6*), but not interleukin-10 (*Il10*), and decreased expression of endothelin-1 (*Edn1*) (Figure 4B-E). Poly(I:C) failed to induce *Il6* in shTLR3 cells, and upregulation of *Cxcl10* was substantially lower in shTLR3 cells. Knockdown of TLR3 alone elevated expression of *Edn1 and Il6*, but not of *Cxcl10* and *Il10*, indicating that TLR3 deficiency promotes a gene expression profile associated with inflammation and vascular remodeling. However, Poly(I:C) stimulation increased *Il10* expression substantially in shTLR3 EC.

Our supplemental data show that transfection of Poly(I:C) increased expression of *Il10, Tlr3* and *Cxcl10* far more than extracellular addition (online supplement Figure E5). This is relevant to our findings, because extracellular addition of Poly(I:C) targets TLR3 via endosomal uptake, whereas liposomal transfection facilitates interaction between Poly(I:C) and both, cytoplasmic and endosomal receptors, increasing synergistic signaling (23).

Copyright © 2018 by the American Thoracic Society

Poly(I:C) treatment restores TLR3 expression in an IL-10 dependent manner.

We then postulated that the release of RNA from damaged cells was insufficient to upregulate TLR3. We found that only high concentration of Poly(I:C) increased expression of *Il10* and *Tlr3* (Figure 4F-G). Blocking IL-10 with a neutralizing antibody abolished TLR3 upregulation after Poly(I:C) treatment (Figure 4H). Consistent with effective IL-10 inhibition, we observed de-repression of CXCL10 (24) (Figure 4I). Poly(I:C) increased activation of nuclear factor-κB (NF-κB) p65 and activator protein 1 (AP-1) c-Jun (Figure 4J), and blocking AP-1 with SR11302 partially blocked Poly(I:C)-induced upregulation of IL-10 (Figure 4K).

Comparison of Poly(I:C) *in vitro* effects in different human endothelial cells

To identify whether different vascular compartments react differently to Poly(I:C) stimulation, we compared the gene expression of human lung microvascular EC (HLMVEC) and human umbilical vein EC (HUVEC). In both cell lines, we found concentration-dependent upregulation of *TLR3*, *DDX58* (RIG-I) and *IFIH1* (MDA-5) (online supplement Figure E6A-B). In HUVEC, Poly(I:C) failed to induce *IL6, CXCL10* and *IL10*, but caused a more substantial induction of *DDX58* and *IFIH1*.

Comparing caspase 3/7 activity of HLMVEC and PAEC, we found that Poly(I:C) caused a concentration-dependent increase in apoptosis only in serum-starved HLMVEC, but not PAEC (online supplement Figure E7A). Because Poly(I:C) increases production of reactive oxygen species (ROS) in systemic endothelium (25), we compared ROS production. We found no difference in Poly(I:C)-induced ROS production between HUVEC and PAEC (online supplement Figure E7B).

Copyright © 2018 by the American Thoracic Society

AJRCCM Articles in Press. Published on 13-September-2018 as 10.1164/rccm.201707-1370OC

dsRNA reduces pulmonary artery remodeling, PH and RV failure *in vivo*

As the loss of TLR3 signaling predisposed to more severe PH we sought to determine in proof-of-principle experiments whether activation of this pathway would prevent the development of PH. First, we tested Poly(I:C) in naive animals. We detected no increase in RVSP and arterial occlusion after treatment with Poly(I:C) (Supplemental Figure E8 A-C). However, we found an increase in MWT and fraction of apoptotic cells in the artery wall after Poly(I:C) treatment (online supplement Figure E8 A, D-F). Then, rats with PH induced by chronic hypoxia were treated with Poly(I:C). In our prophylactic treatment groups, RVSP was significantly lower in rats treated with Poly(I:C). Reduced PH was associated with lower MWT and smaller fraction of fully muscularized arteries (online supplement Figure E9A-F). Poly(I:C) treatment did not significantly compromise echocardiographic right ventricular cardiac output (online supplement Figure E9D) and it ameliorated apoptosis and proliferation in the artery walls (online supplement Figure E9 G-J). Finally, to further explore whether Poly(I:C) reduces severe PH with vascular obliteration, rats with cHx/Su-induced severe PH were treated with Poly(I:C) in prophylactic and interventional strategies. We also tested whether Poly(I:C) treatment had concentration-dependent effects. Prophylactic high dose Poly(I:C) treatment reduced severe cHx/Su PH and vascular occlusion, but had no significant effect on MWT, RV cardiac output or the inflammatory cell profile in the lungs of cHx/Su rats (Figure 5A-F and online supplement Figure E10). We found that only high dose Poly(I:C) had a protective effect (Figure 5A-F). By contrast, low dose Poly(I:C) treatment failed to reduce RVSP and vascular obliteration, but increased MWT. Only high dose Poly(I:C) treatment significantly reduced the fraction of cleaved caspase-3^+ (apoptotic) and proliferating cell nuclear antigen $(PCNA)^+$ (proliferating) cells in the pulmonary arteries (Figure 5G-J). In addition,

Copyright © 2018 by the American Thoracic Society

high dose Poly(I:C) treatment increased IL-10 expression in the lungs of cHx/Su rats (Figure 5K-L). Established severe PH and occlusion was ameliorated by high dose Poly(I:C) (intervention strategy), although muscularization of pulmonary arteries was not significantly reduced (Figure 6A-E). RV cardiac output was improved by Poly(I:C) treatment in established PH (Figure 6F) and similar to the prophylactic strategy, numbers of cleaved caspase-3^+ and $PCNA^+$ pulmonary vascular cells were reduced (Figure 6G-J). To identify the effect of Poly(I:C) treatment on systemic blood vessels, we investigated left ventricular capillary density and apoptotic index. We further found no significant change in the capillary density and apoptotic index in the left ventricle of cHx rats after preventive treatment with high dose Poly(I:C) (online supplement Figure E11). In contrast, we detected increased capillary density and reduced apoptotic index in the left ventricles of cHx/Su rats after therapeutic treatment with high dose Poly(I:C) (online supplement Figure E12).

DISCUSSION

Pulmonary arterial hypertension (PAH) is a devastating disease characterized by progressive narrowing and reorganization of the pulmonary arteries (1; 26). Although increased cell proliferation has been identified in pulmonary vascular lesions, a paradoxical increase in endothelial apoptosis is important for the initiation and progression of the disease (4; 27–30).

In this study, we identify the innate immune receptor TLR3 as a novel regulator of endothelial apoptosis in PAH. Our data show that loss of TLR3 leads to EC apoptosis and that a TLR3 agonist can reduce severe PH in preclinical animal models. There is a well-supported paradigm that pro-inflammatory signaling drives pulmonary vascular

Copyright © 2018 by the American Thoracic Society

AJRCCM Articles in Press. Published on 13-September-2018 as 10.1164/rccm.201707-1370OC

remodeling in PAH. Our data may therefore appear counterintuitive, however there are precedents for protective effects of TLR3 expression and signaling in the systemic circulation and our data imply that this pathway also confers protection in the pulmonary vasculature (1; 12; 31).

We found reduced expression of TLR3 in the lungs and PAEC from PAH patients and we demonstrated an association between loss of TLR3 and caspase-dependent endothelial apoptosis. Extending our *in vitro* studies, we found that TLR3$^{-/-}$ mice have more severe PH and vascular remodeling in response to the cHx/Su protocol, likely caused by increased endothelial apoptosis. Endothelial apoptosis has been implicated in pulmonary vascular remodeling (5; 30; 32) with studies suggesting that early apoptosis contributes to increased vascular cell proliferation in PAH (9; 30; 33–35). Some authors even suggest endothelial apoptosis as a direct cause of PH due to vascular pruning (4; 36). Hence, understanding the mechanism of endothelial apoptosis in PH is important to derive meaningful treatment strategies.

TLR3 is a receptor for a broad spectrum of RNAs, including mRNA released from dying cells and small interfering RNA sequences without regard of the nucleic acid sequence (14–16; 37; 38). Hence RNA is a “damage-associated molecular pattern” for TLR3 during the cellular injury response. TLR3 is mainly localized in the endosomal membrane, but additional receptors for dsRNA and RNA are found in the cytosol, and these include MDA-5 and RIG-I (23; 39; 40). In TLR3-deficient EC, we found that RNA signaling is directed towards these additional RNA receptors, which can induce apoptosis, possibly explaining the higher degree of apoptosis in TLR3-deficient EC. Furthermore, TLR3 knockdown increased expression of endothelin-1 and IL-6, which are implicated in endothelial dysfunction and vascular remodeling (41). Hence, our data

Copyright © 2018 by the American Thoracic Society

indicate that endothelial RNA signaling is dysregulated as a consequence of reduced TLR3 expression. Interestingly, although we show that changes in TLR3 expression impact upon RNA signaling, it is also possible that loss of function polymorphisms of TLR3 could play a role in defective RNA sensing in PAH, similar to a more aggressive clinical phenotype observed in patients with TLR3 polymorphisms in idiopathic pulmonary fibrosis (42).

We then tested whether we can treat PH with dsRNA. Our approach, including dose and regimen of the dsRNA Poly(I:C), was informed by the findings of Cole *et al.*, who showed that Poly(I:C) promoted TLR3 expression and protected from arteriosclerotic vascular injury (12). Our experiments showed that Poly(I:C) treatment prevented and reduced PH, and improved right ventricular failure. Poly(I:C) treatment ameliorated apoptosis, proliferation and remodeling in the pulmonary artery wall in two PH models. Interestingly, Poly(I:C) did not promote pulmonary inflammation in cHx/Su rats. These beneficial effects of TLR3 activation are in contrast to findings by Zimmer *et al*. who showed that Poly(I:C) impaired endothelial function and systemic arterial re-endothelialization after a denuding injury (25). While the study by Zimmer *et al.* investigated Poly(I:C) in an acute model of large scale vascular denudation, we showed protective effects in chronic models of lung vascular remodeling without denuding injury, which could already explain the contrasting results. Further differences are Poly(I:C) dosage and administration route, and it is possible that tissue-specific differences in RNA sensor signaling contribute to the divergent findings. For example, we found that healthy extra-pulmonary EC failed to upregulate IL-10 and CXCL10 in response to Poly(I:C), but had a higher induction of RIG-I and MDA-5 than pulmonary EC. When we observed detrimental effects of Poly(I:C), this was only in the context of an uninjured pulmonary

Copyright © 2018 by the American Thoracic Society

AJRCCM Articles in Press. Published on 13-September-2018 as 10.1164/rccm.201707-1370OC

vasculature. This concept is further supported by the results of a study by Huang and colleagues who found that Poly(I:C) induces *in vitro* barrier dysfunction and cytokine production in healthy lung endothelium (43). The results by George *et al.* also back our notion by showing Poly(I:C)-induced upregulation of endothelin-1 in healthy lung VSMC (44). Taken together, these data imply that endothelial TLR3 expression has a homeostatic role in the context of chronic lung vascular remodeling. Our data further indicate that Poly(I:C) caused no adverse effect on left ventricular capillary density and apoptotic index *in vivo* in both PH models and therapeutic Poly(I:C) treatment was even protective for the left ventricle of cHx/Su rats. Agents to manipulate TLR3 signaling, such as the dsRNA rintatalimod, are available and may exert therapeutic effects on vascular cells in the context of TLR3 deficiency, as we have observed in PH (45).

Our *in vitro* data demonstrated that induction of IL-10 and TLR3 by Poly(I:C) occurred only after high dose treatment. These data imply that high concentrations are therefore required to restore TLR3 levels and reduce apoptosis. This offers a potential explanation of why constitutive RNA signaling fails to offer protection from vascular remodeling; the concentration of RNA internalized following cell injury may simply be too low. Although induction of TLR3 and IL-10 expression by dsRNA has been demonstrated before, induction of TLR3 via IL-10 represents a novel mechanism (12; 17). IL-10 may also explain why Poly(I:C) fails to increase inflammation in cHx/Su rats, as IL-10 reduces inflammation and thereby cardiac remodeling or PH (19; 46; 47). In addition, IL-10 is also produced by circulating endothelial progenitor cells and can stimulate protective natural killer cells (48). Two potential drawbacks exist with our hypothesis that IL-10 mediates protective effects in response to Poly(I:C). First, while Poly(I:C) consistently induced IL-10 in rat lung $CD117^{+}$ EC and in cHx/Su rat lungs, human lung EC showed a less consistent

Copyright © 2018 by the American Thoracic Society

upregulation of IL-10, indicating that Poly(I:C)-induced upregulation of IL-10 may be restricted to subpopulations such as $CD117^+$ EC, or that some of the effects of Poly(I:C) have been mediated through nearby inflammatory cells, which we have not studied in detail in the current work. Second, elevated systemic levels of IL-10 have been reported in PAH patients (49). This may represent the results of insufficient IL-10 signaling in the lung vascular lesions (46; 50).

Further potential limitations of our study are: 1. the use of lung tissue samples from end-stage PAH patients may underestimate the level of apoptosis in active PAH vascular lesions; 2. loss of TLR3 may affect other vascular cells and immune cells.

In conclusion, we provide evidence for loss of TLR3 in pulmonary artery endothelium from patients with advanced PAH. We further show that TLR3 deficiency promotes endothelial apoptosis and exaggerates severe PH in mice. Treatment with dsRNA reduced severe PH in cHx/Su rats, which could depend on induction of TLR3 via IL-10 in EC. These surprising findings indicate that careful manipulation of TLR3 expression and signaling could supplement existing therapeutic approaches for the treatment of PAH.

Copyright © 2018 by the American Thoracic Society

AJRCCM Articles in Press. Published on 13-September-2018 as 10.1164/rccm.201707-1370OC

ACKNOWLEDGEMENTS

AART and the other authors gratefully acknowledge Professor Marlene Rabinovitch (Stanford University) for facilitating experimental work on this project during the BHF-Fulbright award of AART and providing helpful discussion of the research. The authors wish to acknowledge Donatas Kraskauskas, Vita Kraskauskiene, Fiona Morrow and Josephine Pickworth for expert technical support.

Copyright © 2018 by the American Thoracic Society

REFERENCES

1. Rabinovitch, M, Guignabert, C, Humbert, M, Nicolls, MR. Inflammation and immunity in the pathogenesis of pulmonary arterial hypertension. Circ Res 2014; 115: 165-175.

2. Macchia, A, Marchioli, R, Tognoni, G, Scarano, M, Marfisi, R, Tavazzi, L, Rich, S. Systematic review of trials using vasodilators in pulmonary arterial hypertension: why a new approach is needed. Am Heart J 2010; 159: 245-257.

3. Stacher, E, Graham, BB, Hunt, JM, Gandjeva, A, Groshong, SD, McLaughlin, VV, Jessup, M, Grizzle, WE, Aldred, MA, Cool, CD, Tuder, RM. Modern age pathology of pulmonary arterial hypertension. Am J Respir Crit Care Med 2012; 186: 261-272.

4. Chaudhary, KR, Taha, M, Cadete, VJ, Godoy, RS, Stewart, DJ. Proliferative Versus Degenerative Paradigms in Pulmonary Arterial Hypertension: Have We Put the Cart Before the Horse. Circ Res 2017; 120: 1237-1239.

5. Sakao, S, Taraseviciene-Stewart, L, Lee, JD, Wood, K, Cool, CD, Voelkel, NF. Initial apoptosis is followed by increased proliferation of apoptosis-resistant endothelial cells. Faseb j 2005; 19: 1178-1180.

6. Sakao, S, Taraseviciene-Stewart, L, Wood, K, Cool, CD, Voelkel, NF. Apoptosis of pulmonary microvascular endothelial cells stimulates vascular smooth muscle cell growth. Am J Physiol Lung Cell Mol Physiol 2006; 291: L362-8.

7. Reynolds, AM, Xia, W, Holmes, MD, Hodge, SJ, Danilov, S, Curiel, DT, Morrell, NW, Reynolds, PN. Bone morphogenetic protein type 2 receptor gene therapy attenuates hypoxic pulmonary hypertension. Am J Physiol Lung Cell Mol Physiol 2007; 292: L1182-92.

Copyright © 2018 by the American Thoracic Society

AJRCCM Articles in Press. Published on 13-September-2018 as 10.1164/rccm.201707-1370OC

8. Atkinson, C, Stewart, S, Upton, PD, Machado, R, Thomson, JR, Trembath, RC, Morrell, NW. Primary pulmonary hypertension is associated with reduced pulmonary vascular expression of type II bone morphogenetic protein receptor. Circulation 2002; 105: 1672-1678.

9. Tian, W, Jiang, X, Tamosiuniene, R, Sung, YK, Qian, J, Dhillon, G, Gera, L, Farkas, L, Rabinovitch, M, Zamanian, RT, Inayathullah, M, Fridlib, M, Rajadas, J, Peters-Golden, M, Voelkel, NF, Nicolls, MR. Blocking macrophage leukotriene b4 prevents endothelial injury and reverses pulmonary hypertension. Sci Transl Med 2013; 5: 200ra117.

10. Farkas, D, Alhussaini, AA, Kraskauskas, D, Kraskauskiene, V, Cool, CD, Nicolls, MR, Natarajan, R, Farkas, L. Nuclear factor κB inhibition reduces lung vascular lumen obliteration in severe pulmonary hypertension in rats. Am J Respir Cell Mol Biol 2014; 51: 413-425.

11. Tuder, RM, Archer, SL, Dorfmuller, P, Erzurum, SC, Guignabert, C, Michelakis, E, Rabinovitch, M, Schermuly, R, Stenmark, KR, Morrell, NW. Relevant issues in the pathology and pathobiology of pulmonary hypertension. J Am Coll Cardiol 2013; 62: D4-12.

12. Cole, JE, Navin, TJ, Cross, AJ, Goddard, ME, Alexopoulou, L, Mitra, AT, Davies, AH, Flavell, RA, Feldmann, M, Monaco, C. Unexpected protective role for Toll-like receptor 3 in the arterial wall. Proc Natl Acad Sci U S A 2011; 108: 2372-2377.

13. Alexopoulou, L, Holt, AC, Medzhitov, R, Flavell, RA. Recognition of double-stranded RNA and activation of NF-kappaB by Toll-like receptor 3. Nature 2001; 413: 732-738.

Copyright © 2018 by the American Thoracic Society

14. Kariko, K, Ni, H, Capodici, J, Lamphier, M, Weissman, D. mRNA is an endogenous ligand for Toll-like receptor 3. J Biol Chem 2004; 279: 12542-12550.

15. Itoh, K, Watanabe, A, Funami, K, Seya, T, Matsumoto, M. The clathrin-mediated endocytic pathway participates in dsRNA-induced IFN-beta production. J Immunol 2008; 181: 5522-5529.

16. de Bouteiller, O, Merck, E, Hasan, UA, Hubac, S, Benguigui, B, Trinchieri, G, Bates, EE, Caux, C. Recognition of double-stranded RNA by human toll-like receptor 3 and downstream receptor signaling requires multimerization and an acidic pH. J Biol Chem 2005; 280: 38133-38145.

17. Byun, JS, Suh, YG, Yi, HS, Lee, YS, Jeong, WI. Activation of toll-like receptor 3 attenuates alcoholic liver injury by stimulating Kupffer cells and stellate cells to produce interleukin-10 in mice. J Hepatol 2013; 58: 342-349.

18. Thompson, AAR, Arnold, ND, Braithwaite, AT, Casbolt, HL, Pickworth, JA, Cole, JE, Monaco, C, Kiely, D, Sabroe, I, Lawrie, A. Deficiency of Toll-Like Receptor 3 (TLR3) Exacerbates Pulmonary Hypertension in Mice [abstract]. 2016; 193: A3055.

19. Farkas, D, Kraskauskas, D, Kraskauskiene, V, Fowler, AA, Spiegel, S, Farkas, L. Immunomodulatory Therapy With Synthetic Double Stranded Rna prevents Pulmonary Hypertension [abstract]. 2016; 193: A3882.

20. Farkas, D, Cool, C, Goncharova, EA, Farkas, L. Contribution of Reduced Toll-Like Receptor 3 Expression to Endothelial Dysfunction in Pulmonary Hypertension. [abstract]. 2017; 195: A7208.

21. Farkas, D, Kraskauskas, D, Drake, JI, Alhussaini, AA, Kraskauskiene, V, Bogaard, HJ, Cool, CD, Voelkel, NF, Farkas, L. CXCR4 inhibition ameliorates severe obliterative

Copyright © 2018 by the American Thoracic Society

AJRCCM Articles in Press. Published on 13-September-2018 as 10.1164/rccm.201707-1370OC

pulmonary hypertension and accumulation of C-kit$^+$ cells in rats. PLoS One 2014; 9: e89810.

22. Hameed, AG, Arnold, ND, Chamberlain, J, Pickworth, JA, Paiva, C, Dawson, S, Cross, S, Long, L, Zhao, L, Morrell, NW, Crossman, DC, Newman, CMH, Kiely, DG, Francis, SE, Lawrie, A. Inhibition of tumor necrosis factor-related apoptosis-inducing ligand (TRAIL) reverses experimental pulmonary hypertension. J Exp Med 2012; 209: 1919-1935.

23. Palchetti, S, Starace, D, De Cesaris, P, Filippini, A, Ziparo, E, Riccioli, A. Transfected poly(I:C) activates different dsRNA receptors, leading to apoptosis or immunoadjuvant response in androgen-independent prostate cancer cells. J Biol Chem 2015; 290: 5470-5483.

24. Tebo, JM, Kim, HS, Gao, J, Armstrong, DA, Hamilton, TA. Interleukin-10 suppresses IP-10 gene transcription by inhibiting the production of class I interferon. Blood 1998; 92: 4742-4749.

25. Zimmer, S, Steinmetz, M, Asdonk, T, Motz, I, Coch, C, Hartmann, E, Barchet, W, Wassmann, S, Hartmann, G, Nickenig, G. Activation of endothelial toll-like receptor 3 impairs endothelial function. Circ Res 2011; 108: 1358-1366.

26. Rabinovitch, M. Molecular pathogenesis of pulmonary arterial hypertension. J Clin Invest 2012; 122: 4306-4313.

27. Szulcek, R, Happe, CM, Rol, N, Fontijn, RD, Dickhoff, C, Hartemink, KJ, Grunberg, K, Tu, L, Timens, W, Nossent, GD, Paul, MA, Leyen, TA, Horrevoets, AJ, de Man, FS, Guignabert, C, Yu, PB, Vonk-Noordegraaf, A, van Nieuw Amerongen, GP, Bogaard, HJ. Delayed Microvascular Shear Adaptation in Pulmonary Arterial Hypertension. Role of

Copyright © 2018 by the American Thoracic Society

Platelet Endothelial Cell Adhesion Molecule-1 Cleavage. Am J Respir Crit Care Med 2016; 193: 1410-1420.

28. Michelakis, ED. Spatio-temporal diversity of apoptosis within the vascular wall in pulmonary arterial hypertension: heterogeneous BMP signaling may have therapeutic implications. Circ Res 2006; 98: 172-175.

29. Teichert-Kuliszewska, K, Kutryk, MJ, Kuliszewski, MA, Karoubi, G, Courtman, DW, Zucco, L, Granton, J, Stewart, DJ. Bone morphogenetic protein receptor-2 signaling promotes pulmonary arterial endothelial cell survival: implications for loss-of-function mutations in the pathogenesis of pulmonary hypertension. Circ Res 2006; 98: 209-217.

30. Taraseviciene-Stewart, L, Kasahara, Y, Alger, L, Hirth, P, Mc Mahon, G, Waltenberger, J, Voelkel, NF, Tuder, RM. Inhibition of the VEGF receptor 2 combined with chronic hypoxia causes cell death-dependent pulmonary endothelial cell proliferation and severe pulmonary hypertension. Faseb j 2001; 15: 427-438.

31. Abston, ED, Coronado, MJ, Bucek, A, Onyimba, JA, Brandt, JE, Frisancho, JA, Kim, E, Bedja, D, Sung, YK, Radtke, AJ, Gabrielson, KL, Mitzner, W, Fairweather, D. TLR3 deficiency induces chronic inflammatory cardiomyopathy in resistant mice following coxsackievirus B3 infection: role for IL-4. Am J Physiol Regul Integr Comp Physiol 2013; 304: R267-77.

32. Goldthorpe, H, Jiang, JY, Taha, M, Deng, Y, Sinclair, T, Ge, CX, Jurasz, P, Turksen, K, Mei, SH, Stewart, DJ. Occlusive lung arterial lesions in endothelial-targeted, fas-induced apoptosis transgenic mice. Am J Respir Cell Mol Biol 2015; 53: 712-718.

33. Mizuno, S, Farkas, L, Al Husseini, A, Farkas, D, Gomez-Arroyo, J, Kraskauskas, D, Nicolls, MR, Cool, CD, Bogaard, HJ, Voelkel, NF. Severe pulmonary arterial

Copyright © 2018 by the American Thoracic Society

AJRCCM Articles in Press. Published on 13-September-2018 as 10.1164/rccm.201707-1370OC

hypertension induced by SU5416 and ovalbumin immunization. Am J Respir Cell Mol Biol 2012; 47: 679-687.

34. Taraseviciene-Stewart, L, Nicolls, MR, Kraskauskas, D, Scerbavicius, R, Burns, N, Cool, C, Wood, K, Parr, JE, Boackle, SA, Voelkel, NF. Absence of T Cells Confers Increased Pulmonary Arterial Hypertension and Vascular Remodeling. Am J Respir Crit Care Med 2007;

35. Abe, K, Toba, M, Alzoubi, A, Ito, M, Fagan, KA, Cool, CD, Voelkel, NF, McMurtry, IF, Oka, M. Formation of plexiform lesions in experimental severe pulmonary arterial hypertension. Circulation 2010; 121: 2747-2754.

36. Farkas, L, Farkas, D, Ask, K, Moller, A, Gauldie, J, Margetts, P, Inman, M, Kolb, M. VEGF ameliorates pulmonary hypertension through inhibition of endothelial apoptosis in experimental lung fibrosis in rats. J Clin Invest 2009; 119: 1298-1311.

37. Berge, M, Bonnin, P, Sulpice, E, Vilar, J, Allanic, D, Silvestre, JS, Levy, BI, Tucker, GC, Tobelem, G, Merkulova-Rainon, T. Small interfering RNAs induce target-independent inhibition of tumor growth and vasculature remodeling in a mouse model of hepatocellular carcinoma. Am J Pathol 2010; 177: 3192-3201.

38. Cavassani, KA, Ishii, M, Wen, H, Schaller, MA, Lincoln, PM, Lukacs, NW, Hogaboam, CM, Kunkel, SL. TLR3 is an endogenous sensor of tissue necrosis during acute inflammatory events. J Exp Med 2008; 205: 2609-2621.

39. Hornung, V, Ellegast, J, Kim, S, Brzózka, K, Jung, A, Kato, H, Poeck, H, Akira, S, Conzelmann, KK, Schlee, M, Endres, S, Hartmann, G. 5'-Triphosphate RNA is the ligand for RIG-I. Science 2006; 314: 994-997.

40. Asdonk, T, Steinmetz, M, Krogmann, A, Ströcker, C, Lahrmann, C, Motz, I,

Copyright © 2018 by the American Thoracic Society

Paul-Krahe, K, Flender, A, Schmitz, T, Barchet, W, Hartmann, G, Nickenig, G, Zimmer, S. MDA-5 activation by cytoplasmic double-stranded RNA impairs endothelial function and aggravates atherosclerosis. J Cell Mol Med 2016; 20: 1696-1705.

41. Galie, N, Manes, A, Branzi, A. The endothelin system in pulmonary arterial hypertension. Cardiovasc Res 2004; 61: 227-237.

42. O'Dwyer, DN, Armstrong, ME, Trujillo, G, Cooke, G, Keane, MP, Fallon, PG, Simpson, AJ, Millar, AB, McGrath, EE, Whyte, MK, Hirani, N, Hogaboam, CM, Donnelly, SC. The Toll-like receptor 3 L412F polymorphism and disease progression in idiopathic pulmonary fibrosis. Am J Respir Crit Care Med 2013; 188: 1442-1450.

43. Huang, LY, Stuart, C, Takeda, K, D'Agnillo, F, Golding, B. Poly(I:C) Induces Human Lung Endothelial Barrier Dysfunction by Disrupting Tight Junction Expression of Claudin-5. PLoS One 2016; 11: e0160875.

44. George, PM, Badiger, R, Shao, D, Edwards, MR, Wort, SJ, Paul-Clark, MJ, Mitchell, JA. Viral Toll Like Receptor activation of pulmonary vascular smooth muscle cells results in endothelin-1 generation; relevance to pathogenesis of pulmonary arterial hypertension. Biochemical and Biophysical Research Communications 2012; 426: 486-491.

45. Strayer, DR, Carter, WA, Stouch, BC, Stevens, SR, Bateman, L, Cimoch, PJ, Lapp, CW, Peterson, DL, Mitchell, WM. A double-blind, placebo-controlled, randomized, clinical trial of the TLR-3 agonist rintatolimod in severe cases of chronic fatigue syndrome. PLoS One 2012; 7: e31334.

46. Ito, T, Okada, T, Miyashita, H, Nomoto, T, Nonaka-Sarukawa, M, Uchibori, R, Maeda, Y, Urabe, M, Mizukami, H, Kume, A, Takahashi, M, Ikeda, U, Shimada, K,

Copyright © 2018 by the American Thoracic Society

AJRCCM Articles in Press. Published on 13-September-2018 as 10.1164/rccm.201707-1370OC

Ozawa, K. Interleukin-10 expression mediated by an adeno-associated virus vector prevents monocrotaline-induced pulmonary arterial hypertension in rats. Circ Res 2007; 101: 734-741.

47. Krishnamurthy, P, Rajasingh, J, Lambers, E, Qin, G, Losordo, DW, Kishore, R. IL-10 inhibits inflammation and attenuates left ventricular remodeling after myocardial infarction via activation of STAT3 and suppression of HuR. Circ Res 2009; 104: e9-18.

48. Ormiston, ML, Deng, Y, Stewart, DJ, Courtman, DW. Innate immunity in the therapeutic actions of endothelial progenitor cells in pulmonary hypertension. Am J Respir Cell Mol Biol 2010; 43: 546-554.

49. Soon, E, Holmes, AM, Treacy, CM, Doughty, NJ, Southgate, L, Machado, RD, Trembath, RC, Jennings, S, Barker, L, Nicklin, P, Walker, C, Budd, DC, Pepke-Zaba, J, Morrell, NW. Elevated levels of inflammatory cytokines predict survival in idiopathic and familial pulmonary arterial hypertension. Circulation 2010; 122: 920-927.

50. Li, MC, He, SH. IL-10 and its related cytokines for treatment of inflammatory bowel disease. World J Gastroenterol 2004; 10: 620-625.

Copyright © 2018 by the American Thoracic Society

FIGURE LEGENDS

Figure 1. Reduced endothelial TLR3 in lung vascular lesions of patients with PAH. Double immunofluorescence shows strong immunostaining of TLR3 in vWF^+ endothelium in pulmonary artery of control subject (arrows). TLR3 staining is partially lost in endothelium of PAH pulmonary arteries with increased smooth muscle layer and intima thickening. The arrows indicate endothelium with preserved TLR3 expression, whereas asterisks indicate endothelium that is TLR3 deficient. In concentric and plexiform lesions, TLR3 staining is largely lost in vWF^+ endothelium (asterisks). Scale bars: 50 μm (overview on the left), 25 μm (higher detail images). The dotted boxes in the overview images on the left indicate the area that is shown in more detail on the right. Nuclear counterstaining with DAPI.

Figure 2. Reduced TLR3 expression in human PAH and experimental severe PH. (**A**) Lower expression of *TLR3* mRNA in pulmonary artery EC (PAEC) (A, n=4 controls vs. n=3 PAH) from human PAH patients as compared to control subjects without pulmonary vascular disease. (**B-C**) Reduced TLR3 protein expression in PAEC from patients with PAH by Western blot (B). β-actin was used to ensure equal loading of lanes. Semi-quantitative densitometry of TLR3 vs. β-actin confirms reduced TLR3 protein expression in PAEC from PAH patients (C). n=4 different cell lines per group. (**D**) Reduced mRNA expression of TLR3 in the lung tissue from PAH patients (n=5 controls vs. n=6 PAH). (**E-F**) Representative Western blot (E) and semi-quantitative densitometry (F) show reduction of TLR3 protein expression in lung tissue protein lysate from cHx/Su rats at day 21. β-actin was used as loading control. n=3 per group. (**G**) Representative IHC images for TLR3 show less $TLR3^+$ cells (arrows) in endothelial/intima cells in chronic

Copyright © 2018 by the American Thoracic Society

AJRCCM Articles in Press. Published on 13-September-2018 as 10.1164/rccm.201707-1370OC

hypoxia and cHx/Su rats. Counterstaining: Mayer's Hematoxylin. Scale bars: 20 μm. (**H**) Quantification of $TLR3^{+}$ intima cells in pulmonary arteries of cHx and cHx/Su rats. n=3 per group. (**I**) Representative images of vWF and α-SMA IHC show increased pulmonary artery muscularization in $TLR3^{-/-}$ mice exposed to the cHx/Su protocol compared to $TLR3^{+/+}$ wildtype (WT) mice. In contrast, no substantial change occurred in $TLR3^{-/-}$ mice housed in normoxia. Counterstaining with Hematoxylin. Scale bar: 20 μm. (**J-L**) $TLR3^{-/-}$ mice have higher RVSP (J), MWT (K) and fraction of muscularized pulmonary arteries (L) than TLR3 WT mice when exposed to the cHx/Su protocol, but not when exposed to normoxia. n=6-12 (J), 3-7 (K, L). Bars: mean+SEM, scatter plots indicate mean±SEM. **P*<0.05, ***P*<0.01, ****P*<0.0001 (A, C, D: t-test; F, H: One-way ANOVA; J-L: Two-way ANOVA).

Figure 3. Endothelial TLR3 deficiency promotes apoptosis and impairs migration *in vitro*. (**A**) Representative dot plots show increased fraction of Annexin V^{+} (AV) 7-AAD^{-} (apoptotic) cells in PAEC from PAH patients. (**B**) Quantification of AV^{+} 7-AAD^{-} PAEC according to group (n=6 each group). (**C**) Representative dot plots indicate increased fraction of AV^{+} 7-AAD^{-} $CD117^{+}$ rat lung EC after shRNA-mediated knockdown of TLR3. (**D**) Quantification of AV^{+} 7-AAD^{-} $CD117^{+}$ rat lung EC 72h after adenovirus-mediated overexpression of shscrm or shTlr3 (n=3 per group). (**E**) Gene knockdown was confirmed by qRT-PCR of rat *Tlr3* gene mRNA expression 72h after the beginning of the transfection. (**F**) Representative Western blot shows reduction of TLR3 expression in control PAEC 48h after overexpression of cas9 and TLR3 sgRNA (or scramble sgRNA, scrm, as control). β-actin was used as loading control. (**G**) Semi-quantitative densitometry (n=3). (**H**) Immunofluorescence staining for TLR3 shows strong TLR3 expression in scrm

Copyright © 2018 by the American Thoracic Society

CRISPR PAEC, but loss of TLR3 expression in most TLR3 CRISPR PAEC after 72h. The images on the top show an overview (scale bar 50 µm) and the images on the bottom show cells in more detail, with the scrm cells exhibiting a typical cytoplasmic TLR3 staining pattern. (**I**) qRT-PCR shows mRNA expression of *DDX58* (RIG-I) and *IFIH1* (MDA-5) in TLR3 and scrm CRISPR PAEC. (**J**) Representative dot plots show increased fraction of Annexin V^+/7-AAD^- PAEC following serum starvation (basal endothelial growth medium, EGM) and TLR3 knockdown. (**K**) Quantification of AV^+/7-AAD^- PAEC. n=9 per group. (**L**) Representative differential interference contrast (DIC) images of gap closure assay of PAEC after TLR3-targeted or scrm CRISPR. Cells from both groups were treated with vehicle or 100 µM Z-Asp-CH_2-DCB. The images show the damage-free gap at 0h and 15h. The borders of the gaps are indicated by yellow dotted lines. Scale bar: 100 µm. (**M**) Quantification of percent wound closure after 15h (n=9 per group). Mean+SEM. **P*<0.05, ***P*<0.01, ****P*<0.001, *****P*<0.0001 (B, D, E, G, I: t-test; K, M: 2-way ANOVA).

Figure 4. TLR3 deficiency channels endothelial dsRNA signaling through alternate RNA receptors RIG-I and MDA-5 and promotes IL-10 expression in rat lung $CD117^+$ EC. (**A**) Representative optical sections of images acquired by confocal microscopy show that rhodamine-labeled Poly(I:C) (25 µg/ml) localized to TLR3, RIG-I and MDA-5 in shscrm-expressing $CD117^+$ EC with normal TLR3 expression. By contrast, in shTlr3-expressing cells with reduced TLR3 level, Poly(I:C) mainly interacted with RIG-I and MDA-5. Arrows: colocalization of Poly(I:C) and respective receptor. Scale bars: 10 µm. The lower row shows the areas indicated by dotted boxes in the upper row in more detail. Counterstaining with DAPI. (**B-E**) shows changes in the Poly(I:C)-induced mRNA

Copyright © 2018 by the American Thoracic Society

AJRCCM Articles in Press. Published on 13-September-2018 as 10.1164/rccm.201707-1370OC

expression of genes regulating inflammation and vasotonus/remodeling between shscrm- and shTlr3 EC: *Il10* (B), *Edn1* (Endothelin-1, C), *Cxcl10* (CXCL10, D) and *Il6* (E). (**F-G**) Whereas a low dose of Poly(I:C) (0.1 μg/ml) fails to induce *Il10* (F) or *Tlr3* (G) mRNA expression in $CD117^+$ EC, high concentration of Poly(I:C) (50 μg/ml) strongly elevates expression of *Il10* and *Tlr3*. (**H-I**) Poly(I:C)-induced elevation (25 μg/ml) of *Tlr3* expression depends upon IL-10, as treatment with a neutralizing anti-IL-10 antibody (ab) abolishes Poly(I:C)-induced upregulation of *Tlr3* (H), but enhances Poly(I:C)-induced *Cxcl10* upregulation (I). (**J**) Representative Western blots from nuclear lysates show increased nuclear accumulation (activation) of NF-κB p65 and AP-1 c-Jun in Poly(I:C) (25 μg/ml) treated $CD117^+$ EC. Lamin B was used as loading control. (**K**) Inhibition of AP-1 with SR11302 (1 μM) significantly reduces Poly(I:C) (25 μg/ml)-induced IL-10 upregulation. Inhibitor of NF-κB nuclear translocation JSH-23 (25 μM) only resulted in a non-significant trend. All bars: mean+SEM, n=3 per group, except n=3-5 per group for K. **P*<0.05, ***P*<0.01, ****P*<0.001 (One-way ANOVA).

Figure 5. Preventive treatment with high, but not low, dose dsRNA Poly(I:C) reduces severe PH induced by chronic hypoxia and SU5416. (**A**) Diagram of treatment protocol. (**B**) Early high dose (10 mg/kg), but not low dose (1 mg/kg), Poly(I:C) treatment reduces RVSP. n=5 (veh) and 3 [Poly(I:C)] (**C**) High dose early Poly(I:C) treatment did not significantly alter echocardiographic RV cardiac output. n=5 (veh) and 3 [Poly(I:C)]. (**D**) Representative vWF IHC demonstrates occlusion of pulmonary arteries (arrows) in vehicle (veh)- and low Poly(I:C) (1 mg/kg), but not in high Poly(I:C) (10 mg/kg, 3x/week) treated cHx/Su rats after early treatment (day 1-21). (**E-F**) High dose, but not low dose, early Poly(I:C) treatment reduced the fraction of completely occluded small

Copyright © 2018 by the American Thoracic Society

pulmonary arteries (external diameter >25 and <50 μm) (E). In contrast, MWT was not reduced by high dose Poly(I:C) treatment, instead low dose Poly(I:C) increased MWT (F). n=3 per group. (**G-J**) Preventive high dose Poly(I:C) treatment reduced the number of cleaved caspase-3^+ cells (G-H) and $PCNA^+$ cells (I-J) in pulmonary arteries. Low dose Poly(I:C) treatment only had a partial (non-significant) effect on apoptosis and proliferation. n=3 for each group. (**K-L**) Representative Western blot (K) shows increased IL-10 protein expression in the lungs of cHx/Su rats treated with high dose Poly(I:C). β-actin was used as loading control. (L) Semi-quantitative densitometry calculated vs. β-actin and normalized to vehicle. All bars: mean+SEM, scatter plots: mean±SEM. **P*<0.05. Scale bars: 100 μm (D), 20 μm (G, I) (B, E, F, H, J: One-way ANOVA; L: t-test).

Figure 6. Therapeutic high dose Poly(I:C) treatment reduces PH and vascular pathology in the lungs of cHx/Su rats. (**A**) Diagram of the treatment protocol. (**B**) Delayed high dose (10 mg/kg) Poly(I:C) treatment reduced RVSP in cHx/Su rats with established PH (n=6 each group). (**C**) Less occlusion of pulmonary arteries with vWF^+ EC is found after treatment of cHx/Su rats with Poly(I:C) (3x/week, 10 mg/kg) vs. vehicle (veh) after PH was established (day 29-42). (**D**) Histomorphometry revealed that Poly(I:C) treatment reduced the fraction of completely occluded small pulmonary arteries (n=3-4 per group). (**E**) There was no change however in MWT of small pulmonary arteries with Poly(I:C) treatment (n=3 per group). (**F**) Late Poly(I:C) treatment improved RV cardiac output as measured by echocardiography [veh n=6, Poly(I:C) n=7]. (**G-J**) Therapeutic Poly(I:C) treatment decreased the fraction of cleaved caspase-3^+ cells (G-H) and $PCNA^+$ cells (I-J) in the pulmonary artery wall [n=3 per group, except n=4 for PCNA Poly(I:C)]. Bars: mean+SEM, scatter plots: mean±SEM. **P*<0.05, ***P*<0.01, ****P*<0.001. Scale bar:

Copyright © 2018 by the American Thoracic Society

AJRCCM Articles in Press. Published on 13-September-2018 as 10.1164/rccm.201707-1370OC

100 μm (C), 20 μm (G, I) (B, E, F, H, J: t-test; D: One-way ANOVA).

Copyright © 2018 by the American Thoracic Society

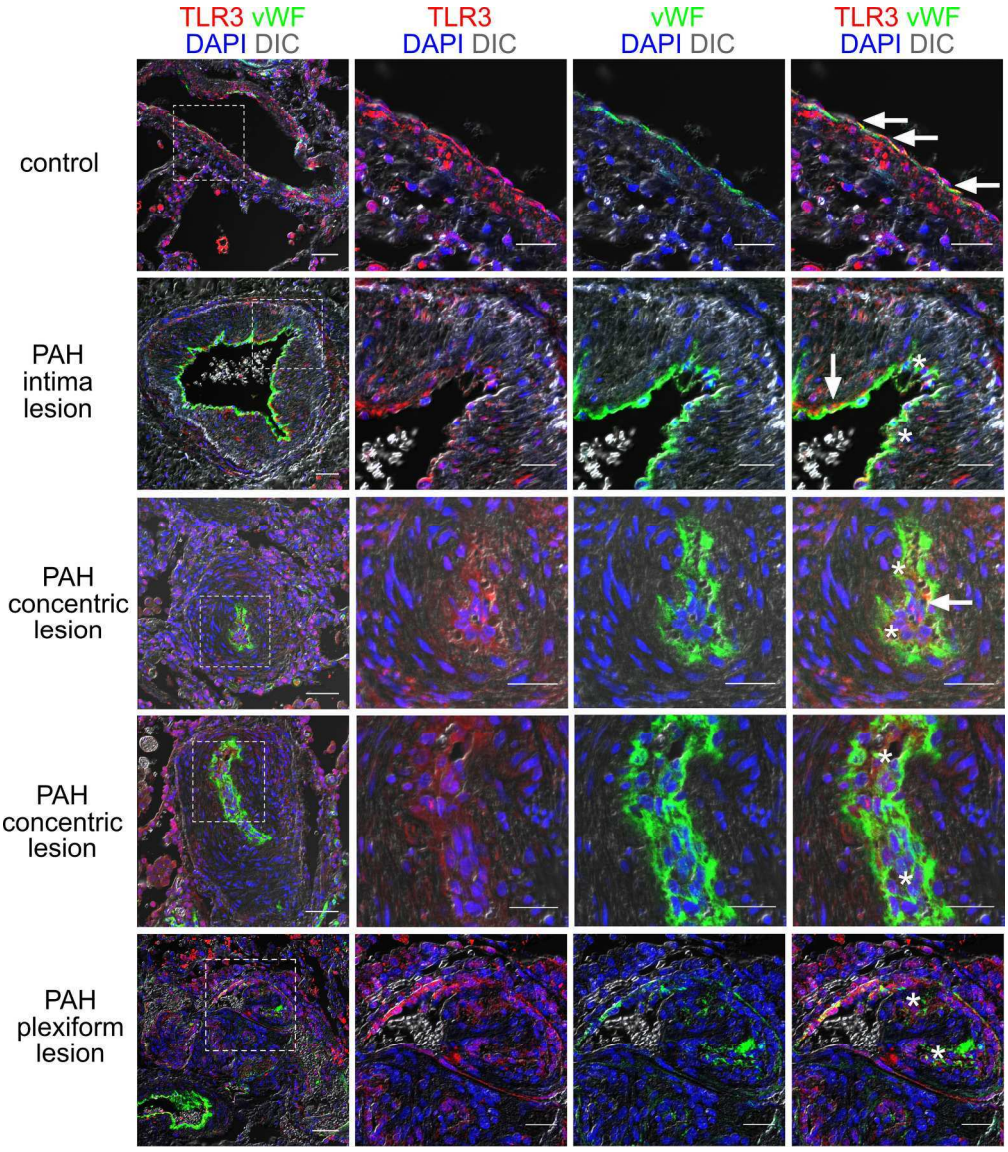

Figure 1. Reduced endothelial TLR3 in lung vascular lesions of patients with PAH. Double immunofluorescence shows strong immunostaining of TLR3 in vWF^+ endothelium in pulmonary artery of control subject (arrows). TLR3 staining is partially lost in endothelium of PAH pulmonary arteries with increased smooth muscle layer and intima thickening. The arrows indicate endothelium with preserved TLR3 expression, whereas asterisks indicate endothelium that is TLR3 deficient. In concentric and plexiform lesions, TLR3 staining is largely lost in vWF^+ endothelium (asterisks). Scale bars: 50 µm (overview on the left), 25 µm (higher detail images). The dotted boxes in the overview images on the left indicate the area that is shown in more detail on the right. Nuclear counterstaining with DAPI.

212x241mm (300 x 300 DPI)

Copyright © 2018 by the American Thoracic Society

AJRCCM Articles in Press. Published on 13-September-2018 as 10.1164/rccm.201707-1370OC

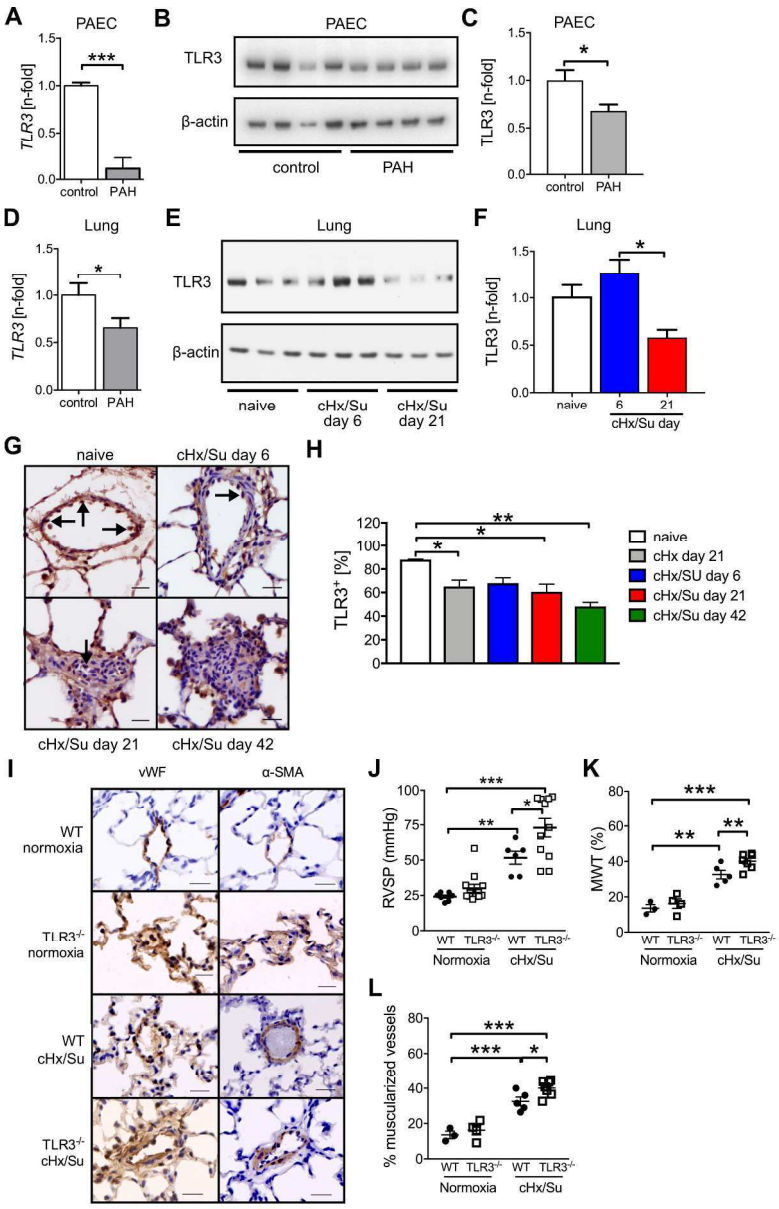

Figure 2. Reduced TLR3 expression in human PAH and experimental severe PH. (**A**) Lower expression of TLR3 mRNA in pulmonary artery EC (PAEC) (A, n=4 controls vs. n=3 PAH) from human PAH patients as compared to control subjects without pulmonary vascular disease. (**B-C**) Reduced TLR3 protein expression in PAEC from patients with PAH by Western blot (B). β-actin was used to ensure equal loading of lanes. Semi-quantitative densitometry of TLR3 vs. β-actin confirms reduced TLR3 protein expression in PAEC from PAH patients (C). n=4 different cell lines per group. (**D**) Reduced mRNA expression of TLR3 in the lung tissue from PAH patients (n=5 controls vs. n=6 PAH). (**E-F**) Representative Western blot (E) and semi-quantitative densitometry (F) show reduction of TLR3 protein expression in lung tissue protein lysate from cHx/Su rats at day 21. β-actin was used as loading control. n=3 per group. (**G**) Representative IHC images for TLR3 show less $TLR3^{+}$ cells (arrows) in endothelial/intima cells in chronic hypoxia and cHx/Su rats. Counterstaining: Mayer's Hematoxylin. Scale bars: 20 μm. (**H**) Quantification of $TLR3^{+}$ intima cells in pulmonary arteries of cHx and cHx/Su rats. n=3 per group. (**I**) Representative images of vWF and α-SMA IHC show increased pulmonary artery muscularization in $TLR3^{-/-}$ mice exposed to the cHx/Su protocol

Copyright © 2018 by the American Thoracic Society

compared to $TLR3^{+/+}$ wildtype (WT) mice. In contrast, no substantial change occurred in $TLR3^{-/-}$ mice housed in normoxia. Counterstaining with Hematoxylin. Scale bar: 20 μm. (**J-L**) $TLR3^{-/-}$ mice have higher RVSP (J), MWT (K) and fraction of muscularized pulmonary arteries (L) than TLR3 WT mice when exposed to the cHx/Su protocol, but not when exposed to normoxia. n=6-12 (J), 3-7 (K, L). Bars: mean+SEM, scatter plots indicate mean±SEM. **P*<0.05, ***P*<0.01, ****P*<0.0001 (A, C, D: t-test; F, H: One-way ANOVA; J-L: Two-way ANOVA).

212x327mm (300 x 300 DPI)

Copyright © 2018 by the American Thoracic Society

AJRCCM Articles in Press. Published on 13-September-2018 as 10.1164/rccm.201707-1370OC

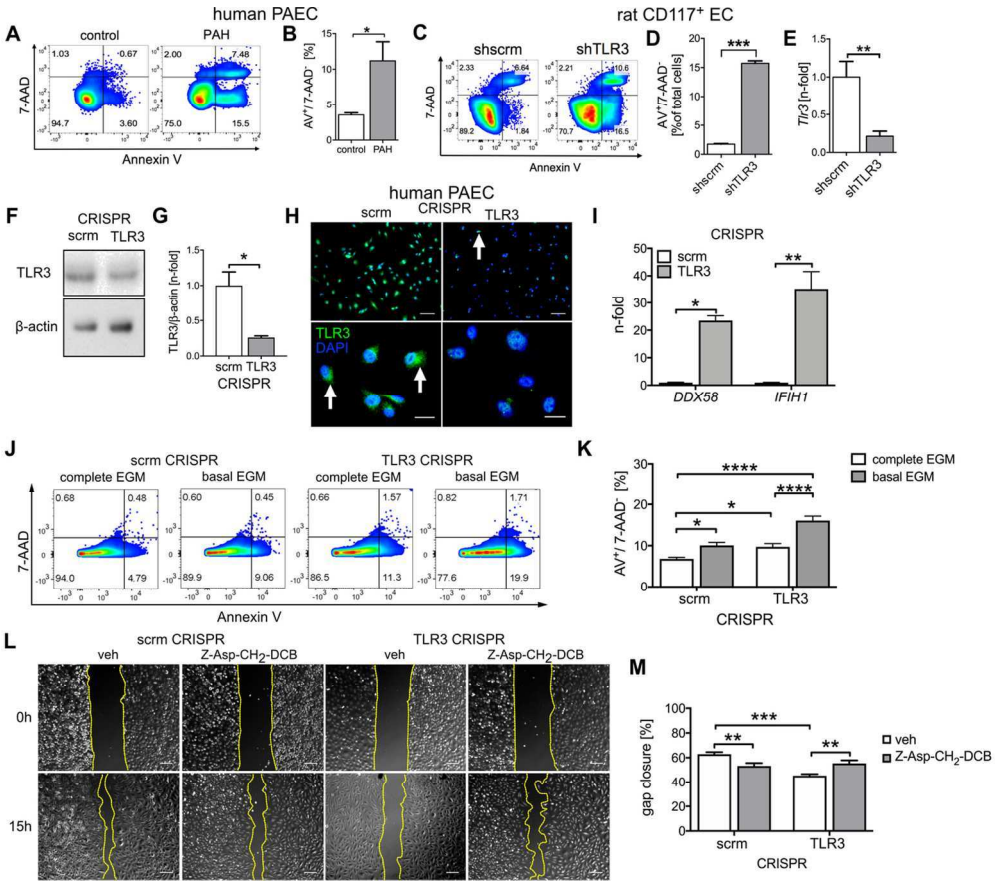

Figure 3. Endothelial TLR3 deficiency promotes apoptosis and impairs migration in vitro. (**A**) Representative dot plots show increased fraction of Annexin V^+ (AV) 7-AAD^- (apoptotic) cells in PAEC from PAH patients. (**B**) Quantification of AV^+ 7-AAD^- PAEC according to group (n=6 each group). (**C**) Representative dot plots indicate increased fraction of AV^+ 7-AAD^- $CD117^+$ rat lung EC after shRNA-mediated knockdown of TLR3. (**D**) Quantification of AV^+ 7-AAD- $CD117^+$ rat lung EC 72h after adenovirus-mediated overexpression of shscrm or shTlr3 (n=3 per group). (**E**) Gene knockdown was confirmed by qRT-PCR of rat *Tlr3* gene mRNA expression 72h after the beginning of the transfection. (**F**) Representative Western blot shows reduction of TLR3 expression in control PAEC 48h after overexpression of cas9 and TLR3 sgRNA (or scramble sgRNA, scrm, as control). β-actin was used as loading control. (**G**) Semi-quantitative densitometry (n=3). (**H**) Immunofluorescence staining for TLR3 shows strong TLR3 expression in scrm CRISPR PAEC, but loss of TLR3 expression in most TLR3 CRISPR PAEC after 72h. The images on the top show an overview (scale bar 50 µm) and the images on the bottom show cells in more detail, with the scrm cells exhibiting a typical cytoplasmic TLR3 staining pattern. (**I**) qRT-PCR shows mRNA expression of *DDX58* (RIG-I) and *IFIH1* (MDA-5) in TLR3 and scrm CRISPR PAEC. (**J**) Representative dot plots show increased fraction of Annexin V^+/7-AAD^- PAEC following serum starvation (basal endothelial growth medium, EGM) and TLR3 knockdown. (**K**) Quantification of AV^+/7-AAD^- PAEC. n=9 per group. (**L**) Representative differential interference contrast (DIC) images of gap closure assay of PAEC after TLR3-targeted or scrm CRISPR. Cells from both groups were treated with vehicle or 100 µM Z-Asp-CH_2-DCB. The images show the damage-free gap at 0h and 15h. The borders of the gaps are indicated by yellow dotted lines. Scale bar: 100 µm. (**M**) Quantification of percent wound closure after 15h (n=9 per group). Mean+SEM. **P*<0.05, ***P*<0.01, ****P*<0.001, *****P*<0.0001 (B, D, E, G, I: t-test; K, M: 2-way ANOVA).

125x109mm (300 x 300 DPI)

Copyright © 2018 by the American Thoracic Society

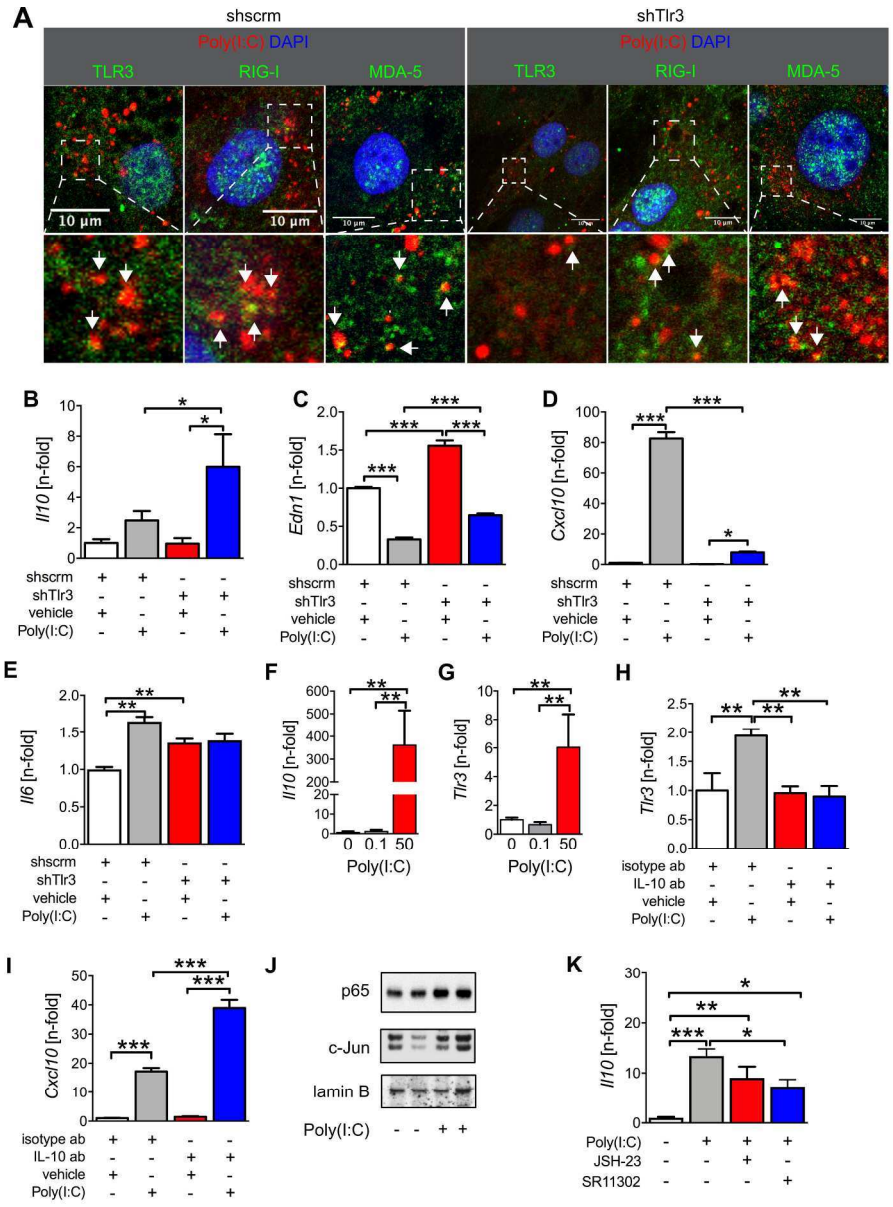

Figure 4. TLR3 deficiency channels endothelial dsRNA signaling through alternate RNA receptors RIG-I and MDA-5 and promotes IL-10 expression in rat lung CD117$^+$ EC. (**A**) Representative optical sections of images acquired by confocal microscopy show that rhodamine-labeled Poly(I:C) (25 µg/ml) localized to TLR3, RIG-I and MDA-5 in shscrm-expressing CD117$^+$ EC with normal TLR3 expression. By contrast, in shTlr3-expressing cells with reduced TLR3 level, Poly(I:C) mainly interacted with RIG-I and MDA-5. Arrows: colocalization of Poly(I:C) and respective receptor. Scale bars: 10 µm. The lower row shows the areas indicated by dotted boxes in the upper row in more detail. Counterstaining with DAPI. (**B-E**) shows changes in the Poly(I:C)-induced mRNA expression of genes regulating inflammation and vasotonus/remodeling between shscrm- and shTlr3 EC: *Il10* (B), *Edn1* (Endothelin-1, C), *Cxcl10* (CXCL10, D) and *Il6* (E). (**F-G**) Whereas a low dose of Poly(I:C) (0.1 µg/ml) fails to induce *Il10* (F) or *Tlr3* (G) mRNA expression in CD117$^+$ EC, high concentration of Poly(I:C) (50 µg/ml) strongly elevates expression of *Il10* and *Tlr3*. (**H-I**) Poly(I:C)-induced elevation (25 µg/ml) of Tlr3 expression depends upon IL-10, as treatment with a neutralizing anti-IL-10 antibody (ab) abolishes Poly(I:C)-induced upregulation of Tlr3 (H), but

Copyright © 2018 by the American Thoracic Society

AJRCCM Articles in Press. Published on 13-September-2018 as 10.1164/rccm.201707-1370OC

enhances Poly(I:C)-induced Cxcl10 upregulation (I). (**J**) Representative Western blots from nuclear lysates show increased nuclear accumulation (activation) of NF-κB p65 and AP-1 c-Jun in Poly(I:C) (25 μg/ml) treated $CD117^{+}$ EC. Lamin B was used as loading control. (**K**) Inhibition of AP-1 with SR11302 (1 μM) significantly reduces Poly(I:C) (25 μg/ml)-induced IL-10 upregulation. Inhibitor of NF-κB nuclear translocation JSH-23 (25 μM) only resulted in a non-significant trend. All bars: mean+SEM, n=3 per group, except n=3-5 per group for K. **P*<0.05, ***P*<0.01, ****P*<0.001 (One-way ANOVA).

212x285mm (300 x 300 DPI)

Copyright © 2018 by the American Thoracic Society

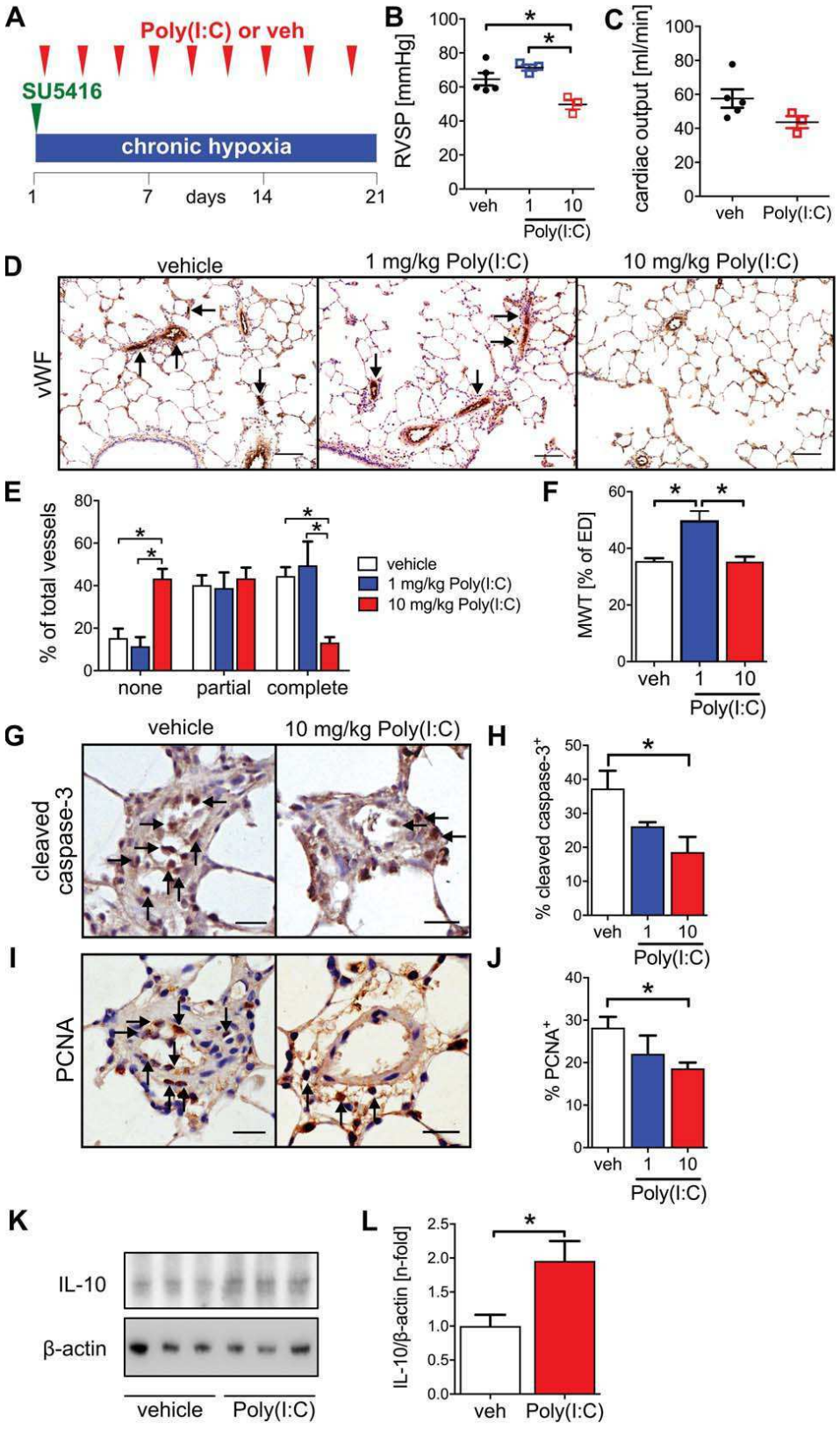

Figure 5. Preventive treatment with high, but not low, dose dsRNA Poly(I:C) reduces severe PH induced by chronic hypoxia and SU5416. **A.** Diagram of treatment protocol. **B.** Early high dose (10 mg/kg), but not low dose (1 mg/kg), Poly(I:C) treatment reduces RVSP. n=5 (veh) and 3 [Poly(I:C)] **C.** High dose early Poly(I:C) treatment did not significantly alter echocardiographic RV cardiac output. n=5 (veh) and 3 [Poly(I:C)]. **D.** Representative vWF IHC demonstrates occlusion of pulmonary arteries (arrows) in vehicle (veh)- and low Poly(I:C) (1 mg/kg), but not in high Poly(I:C) (10 mg/kg, 3x/week) treated cHx/Su rats after early treatment (day 1-21). **E-F.** High dose, but not low dose, early Poly(I:C) treatment reduced the fraction of completely occluded small pulmonary arteries (external diameter >25 and <50 μm) (E). In contrast, MWT was not reduced by high dose Poly(I:C) treatment, instead low dose Poly(I:C) increased MWT (F). n=3 per group. **G-J.** Preventive high dose Poly(I:C) treatment reduced the number of cleaved caspase-3$^+$ cells (G-H) and PCNA$^+$ cells (I-J) in pulmonary arteries. Low dose Poly(I:C) treatment only had a partial (non-significant) effect on apoptosis and proliferation. n=3 for each group. **K-L.** Representative Western blot (K) shows increased IL-10 protein expression in the lungs of cHx/Su rats treated with high dose Poly(I:C). β-actin was used as loading control. (L) Semi-quantitative densitometry calculated vs. β-actin and normalized to vehicle. All bars: mean+SEM, scatter plots: mean±SEM. *P<0.05. Scale bars: 100 μm (D), 20 μm (G, I) (B, E, F, H, J: One-way ANOVA; L: t-test).

Copyright © 2018 by the American Thoracic Society

AJRCCM Articles in Press. Published on 13-September-2018 as 10.1164/rccm.201707-1370OC

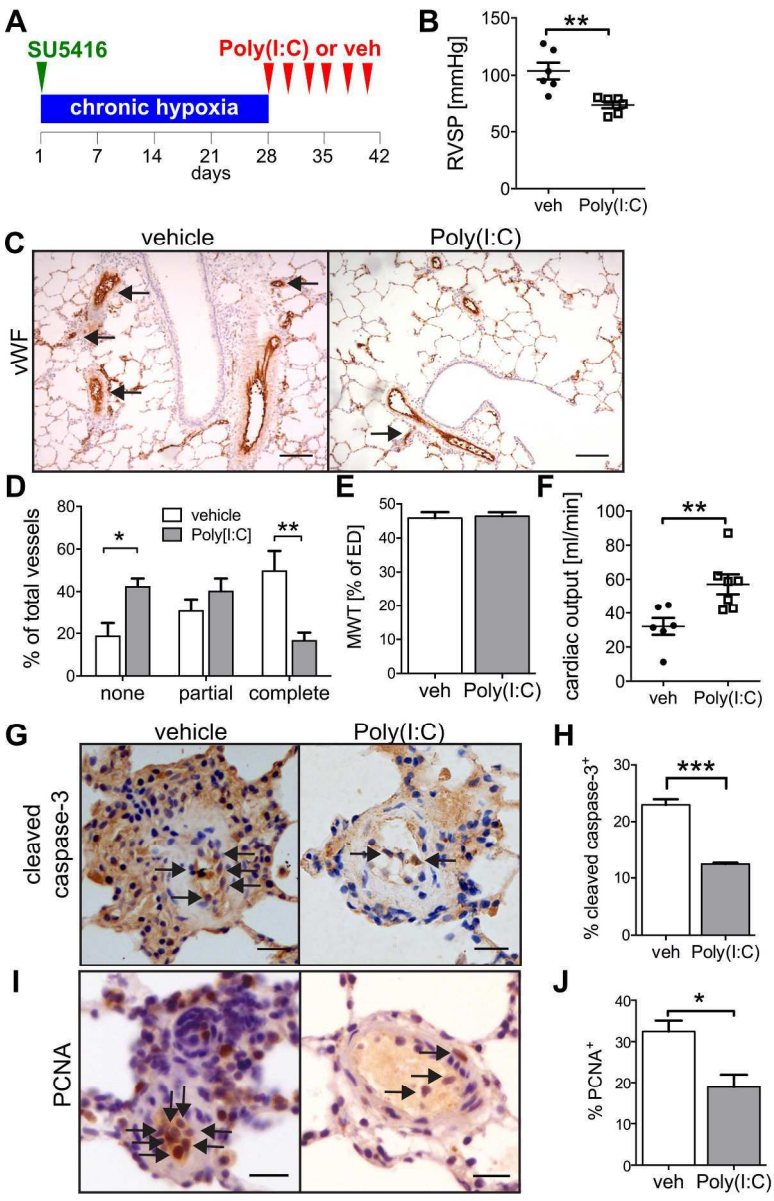

Figure 6. Therapeutic high dose Poly(I:C) treatment reduces PH and vascular pathology in the lungs of cHx/Su rats. (**A**) Diagram of the treatment protocol. (**B**) Delayed high dose (10 mg/kg) Poly(I:C) treatment reduced RVSP in cHx/Su rats with established PH (n=6 each group). (**C**) Less occlusion of pulmonary arteries with vWF+ EC is found after treatment of cHx/Su rats with Poly(I:C) (3x/week, 10 mg/kg) vs. vehicle (veh) after PH was established (day 29-42). (**D**) Histomorphometry revealed that Poly(I:C) treatment reduced the fraction of completely occluded small pulmonary arteries (n=3-4 per group). (**E**) There was no change however in MWT of small pulmonary arteries with Poly(I:C) treatment (n=3 per group). (**F**) Late Poly(I:C) treatment improved RV cardiac output as measured by echocardiography [veh n=6, Poly(I:C) n=7]. (**G-J**) Therapeutic Poly(I:C) treatment decreased the fraction of cleaved caspase-3^+ cells (G-H) and $PCNA^+$ cells (I-J) in the pulmonary artery wall [n=3 per group, except n=4 for PCNA Poly(I:C)]. Bars: mean+SEM, scatter plots: mean±SEM. *P<0.05, **P<0.01, ***P<0.001. Scale bar: 100 μm (C), 20 μm (G, I) (B, E, F, H, J: t-test; D: One-way ANOVA).

Copyright © 2018 by the American Thoracic Society

AJRCCM Articles in Press. Published on 13-September-2018 as 10.1164/rccm.201707-1370OC

ONLINE DATA SUPPLEMENT

Toll-like receptor 3 is a therapeutic target for Pulmonary Hypertension

Daniela Farkas *, A. A. Roger Thompson *, Aneel R. Bhagwani, Schuyler Hultman, Hyun Ji, Naveen Kotha, Grant Farr, Nadine D. Arnold, Adam Braithwaite, Helen Casbolt, Jennifer E. Cole, Ian Sabroe, Claudia Monaco, Carlyne D. Cool, Elena A. Goncharova, Allan Lawrie, Laszlo Farkas

* These authors contributed equally

Copyright © 2018 by the American Thoracic Society

AJRCCM Articles in Press. Published on 13-September-2018 as 10.1164/rccm.201707-1370OC

DETAILED METHODS

Animal models and strains

For chronic hypoxia (cHx) exposure, male animals were placed in a normobaric nitrogen dilution chamber (inspiratory oxygen fraction 10%) and for 21 days. The following strains were used: Sprague Dawley rats (Envigo laboratories, Indianapolis, IN), C57BL/6 mice (Jackson Laboratories, Bar Harbor, ME) and TLR3 knockout mouse strain B6;129S1-*Tlr3tm1Flv*/J (C57BL/6 background) (sources: Prof. Claudia Monaco, University of Oxford, UK and Jackson Laboratories). The cHx/Su model was employed as published previously (E1; E2): male Sprague Dawley rats received a single subcutaneous (s.c.) injection of SU5416 (20 mg/kg, Millipore-Sigma, St. Louis, MO). Mice were housed in cHx for 21 days with weekly s.c. injections of SU5416 (20 mg/kg) as published by Ciuclan et al. (E3). Rats were exposed to cHx for 1, 6 (early study part) and 21 days (preventive treatment strategy) and 28 days (therapeutic treatment strategy). In the therapeutic treatment strategy, exposure to cHx for 28 days was followed by 14 days of housing in normoxia (room air).

Note on TLR3 WT mice used in this study

$TLR3^{-/-}$ mice are available commercially as homozygous knockout animals on a C57BL/6 background and the controls recommended by the supplier (Jackson Labs) are wildtype C57BL/6 mice, which we used in our study. Generating $TLR3^{+/+}$ littermates would have required several generations of backcrosses between $TLR3^{-/-}$ and C57BL/6 mice.

Copyright © 2018 by the American Thoracic Society

AJRCCM Articles in Press. Published on 13-September-2018 as 10.1164/rccm.201707-1370OC

Isolation of rat CD117$^+$ endothelial cells

Because of our previous publication that suggests an important contribution of CD117$^+$ EC to the occlusive pulmonary arteriopathy that is characteristic of cHx/Su rats (E2), we isolated CD117$^+$ EC from the lung periphery of naive adult Sprague Dawley rats (8-10 weeks, Envigo laboratories). After resection, a lung single cell suspension was prepared using a modified protocol according to van Beijnum et al. (E4). In short, lung tissue was dissected into <1mm^3 pieces followed by enzymatic digestion with digested in 0.1% collagenase II/ 2.5 U/ml dispase solution (both from Thermo Fisher Scientific, Waltham, MA) for 30 min at 37˚C. This was followed by another incubation with 0.1% DNase (Sigma-Aldrich, St. Louis, MO) for 30 minutes at 37˚C. CD117$^+$ cells were obtained by immunomagnetic sorting using magnets and the "FITC Any Species positive selection" kit from Stem Cell Technologies (Vancouver, BC). Then, hematopoieitic cells were depleted from the cell pool by negative sorting with bead-conjugated antibodies directed against CD5, CD11b/c and CD45 (pan-CD45) using Pluribeads (Pluribeads, Leipzig, Germany) according to the manufacturer's recommendation. To enrich the endothelial fraction, CD31$^+$ cells were selected from these CD117$^+$ and hematopoietic lineage negative (lin$^-$) cells using pluribeads. The hereby obtained CD117$^+$ lin$^-$ CD31$^+$ cells (CD117$^+$ EC) were cultured on type I collagen coated dishes with EGM-2MV medium (Lonza, Walkersville, MD) in a humidified cell incubator at 37˚C and 5% CO2.

Characterization of CD117$^+$ endothelial cells

CD117$^+$ EC were characterized by flow cytometry according to standard protocols for expression of EC marker von Willebrand Factor (vWF) and lack of hematopoietic

Copyright © 2018 by the American Thoracic Society

AJRCCM Articles in Press. Published on 13-September-2018 as 10.1164/rccm.201707-1370OC

markers CD45 and CD11b/c using a FACS Canto (BD Biosciences), in the Flow cytometry Core facility at VCU (see section on flow cytometry for further details). For functional characterization, angiogenic tube formation assay was performed by seeding 2×10^4 $CD117^+$ EC per well in EGM-2MV on matrigel (BD Biosciences) on a 96 well plate. In addition, the clonal expansion potential was determined by a clonal expansion assay: $CD117^+$ EC were seeded at a limiting dilution of 1 cell per well in 96 well plates. Then, the growth of clonal colonies was identified by differential interference contrast (DIC) microscopy after 7 days using an Olympus IX70 inverted microscope with CellSens software (both Olympus, Waltham, MD).

Human lung microvascular EC (HLMVEC)

HLMVEC were isolated from explanted lung tissue by CD31 magnetic bead selection (Dynabeads, Thermo Fisher Scientific).

Human umbilical vein EC (HUVEC)

HUVEC pooled from several donors were obtained from a commercial vendor (Lonza Clonetics, Walkersville, MD).

Cell culture experiments

Human pulmonary artery EC (PAEC), HLMVEC and HUVEC

PAEC and HUVEC were cultured with complete EGM-2 medium (Lonza, Walkersville, MD and Promocell, Heidelberg, Germany), and HLMVEC were grown in basal media supplemented with endothelial cell growth supplement (ScienCell

Copyright © 2018 by the American Thoracic Society

AJRCCM Articles in Press. Published on 13-September-2018 as 10.1164/rccm.201707-1370OC

Research Laboratories Inc, Carlsbad, CA), 5% foetal bovine serum and penicillin/streptomycin. For apoptosis assay and baseline TLR3 expression, cells were removed after 24h for flow cytometry for Annexin V binding or for quantitative real-time PCR (qRT-PCR). For Western blot, cells were grown on 10 cm dishes until subconfluency and protein isolation and Western blots were prepared as indicated under Western blotting.

CRISPR gene editing

For Clustered Regularly Interspaced Short Palindromic Repeats (CRISPR) interference, PAEC were transfected with 100 multiplicity of infection (MOI) of adenovirus encoding Cas9 nuclease (Ad-CMV-Cas9, Vector Biolabs, Malvern, PA) and multiplicity of infection (MOI) 100 of adenovirus encoding a single guidance RNA (sgRNA) targeting a 20 base sequence in exon 2 of human TLR3 (Ad-TLR3-sgRNA-CRISPRi) or scrambled control sgRNA (Ad-scrm-sgRNA-CRISPRi) (both Applied Biological Materials, Richmond, BC, Canada). Similar co-transfection approaches using two viral vectors expressing Cas9 and sgRNA have been used successfully in other cell lines (E5; E6). The virus was removed after 16 hours. Knockout efficiency was confirmed using Western blot and immunocytochemistry. We did not select for knockout clones, because the PAEC cultures were in average in passage 5 or 6 at transfection and we have observed in previous experiments that during selection and expansion, EC will likely reach a critical number of population doublings and become growth-arrested.

Copyright © 2018 by the American Thoracic Society

AJRCCM Articles in Press. Published on 13-September-2018 as 10.1164/rccm.201707-1370OC

Immunocytochemistry

For immunocytochemistry to detect TLR3, a protocol similar to a previously published protocol was used (E7). In brief, PAEC were passaged after CRISPR and grown on LabTek chamber slides (Nalgene NUNC, ThermoFisher Scientific, Rochester, NY). For staining, cells were fixed with 10% formalin for 10 min. Then cells were permeabilized with 0.5 Triton-X for 10 min and blocked with 1% BSA for 30 min. The cells were incubated with the primary antibody (anti-TLR3, LS Bioscience) in 1% BSA overnight at 4℃. Then, cells were incubated with AF488 -labeled secondary antibody (ThermoFisher Scientific) for 1h and counterstained with DAPI. The stained slides were mounted with slowfade and imaged with Olympus IX70 inverted microscope and CellSens software. Images were assembled with Fiji software (E8).

Serum starvation

For serum starvation, cells were cultured in basal growth media (no FBS, no growth factors) for 24h. Annexin V staining and analysis were performed as described under flow cytometry.

Migration/gap closure assay

For migration/gap closure assay, Ibidi chambers with defined cell-free gaps were used (Ibidi, Madison, WI). In brief, scrm and TLR3 CRISPRi cells were seeded in 6 well plates at 5000 cells/cm^2 and grown until confluent. The divider was removed, leaving a defined cell-free gap. Cells were cultured with complete EGM2 or, for serum starvation experiments, with basal EGM (no FBS, no growth factors). Images were obtained at 0h

Copyright © 2018 by the American Thoracic Society

AJRCCM Articles in Press. Published on 13-September-2018 as 10.1164/rccm.201707-1370OC

and 15h after initiating the gap closure with an Olympus IX70 inverted microscope and CellSens software. During the gap closure period, the cells were treated with 100 μM (3S)-5-(2,6-dichlorobenzoyl)oxy-4-oxo-3-(phenylmethoxycarbonylamino) pentanoic acid (Z-Asp-CH2-DCB) (Bachem, Torrance, CA) or vehicle. Measurements were performed using Fiji software (E8). Analysis was done according to a modified protocol similar to Yue et al. (E9).

Caspase 3/7 activity and reactive oxygen species activity.

Caspase activity was determined using Capase-Glo 3/7 (Promega, Madison, WI) and normalized for cell number using CellTiter-Glo (Promega). Reactive oxygen species (ROS) were measured using ROS-Glo (Promega) and normalized for cell number using CellTiter-Glo. Values are given as n-fold vs. control samples. Luminescence was measured using a Synergy H1 plate reader (BioTek, Winooski, VT) or a GloMax Explorer luminiscence plater reader (Promega).

Rat CD117$^+$ endothelial cell experiments

Rat CD117$^+$ EC were cultured with EGM-2MV medium and seeded at 3000 cells/cm^2 in 6 well plates for experiments. Cells were stimulated with the following conditions: extracellular addition of Poly(I:C) (Tocris, Minneapolis, MN) at 0.1, 25 or 50 μg/ml for 24h, transfection of Poly(I:C) at 2 μg/ml, neutralizing polyclonal goat anti-rat-IL-10 antibody at 1 μg/ml (R&D Systems, Minneapolis, MN), SR11302 at 1 μM (Tocris), JSH-23 at 25 μM (Santa Cruz Biotechnology, Santa Cruz, CA). For transfection of Poly(I:C), Effectene transfection reagent (Qiagen, Germantown, MD) was used, combining 2 μg

Copyright © 2018 by the American Thoracic Society

AJRCCM Articles in Press. Published on 13-September-2018 as 10.1164/rccm.201707-1370OC

Poly(I:C), 16 µl enhancer and 20 µl Effectene reagent per 1 ml of culture media. To overexpress single hairpin (sh) RNA directed against rat TLR3 or scrambled (control) shRNA in $CD117^+$ EC, Ad-r-shTLR3 and Ad-shscrm adenoviruses were obtained from Vector Biolabs (Malvern, PA). $CD117^+$ EC were incubated with adenoviruses at MOI of 50 for 16h, then adenovirus was removed and fresh media added. After 72h, gene knockdown was verified and cells were stimulated with Poly(I:C) or vehicle.

For immunocytochemistry/stimulation with rhodamine-labelled Poly(I:C), cells were seeded at 5000/cm^2 in µ-Slide VI 0.4 chambers (Ibidi, Madison, WI) according to the manufacturer's recommendation. TLR3 knockdown was established by transfection with Ad-r-shTLR3 (control: Ad-shscrm) as described above. 72h after initial adenovirus inoculation, 25 ng/ml rhodamine-labeled Poly(I:C) (Invivogen, San Diego, CA) was added to all wells for 24h. Then, media was removed and cells were fixed with 10% formalin/phosphate-buffered saline (PBS) for 10 min at room temperature. Then, the cells were permeabilized with 0.5% Triton-X/PBS for 10 min at room temperature, followed by blocking with 1% bovine serum albumin (BSA)/PBS for 30 min. The cells were incubated with the primary antibodies anti-TLR3 (LifeSpan Biosciences, Seattle, WA), anti-RIG-I (Abcam, Cambridge, MA) and anti-MDA-5 (LifeSpan Biosciences) dissolved in 1% BSA/PBS overnight at 4˚C. Then, the cells were incubated with AF647-labeled secondary antibodies (Invitrogen, Carlsbad, CA) in 1%BSA/PBS for 1 h at room temperature, followed by counterstaining with 4',6-diamidino-2-phenylindole (DAPI, Invitrogen). Images were acquired with a Zeiss LSM710 confocal microscope and Zen software (Zeiss, Peabody, MA), located in the Microscopy Core Facility at Virginia Commonwealth University. Images were assembled in Fiji.

Copyright © 2018 by the American Thoracic Society

AJRCCM Articles in Press. Published on 13-September-2018 as 10.1164/rccm.201707-1370OC

Quantitative real-time polymerase chain reaction (qRT-PCR)

RNA isolation was carried out using the RNeasy isolation kit (Qiagen, Germantown, MD) or the Quick RNA mini-prep (Zymo Research, Irvine, CA) according to the manufacturer's recommendation. For transcription of RNA to cDNA, RNA first underwent treatment with DNase I (Invitrogen, Thermo Fisher Scientific, Waltham, MD) for 15 min at room temperature, followed by inactivation of DNase with Ethylenediaminetetraacetic acid and incubation at 65˚C for 10 min. The reverse transcriptase (RT) reaction was done with the High capacity RT reaction kit (Applied Biosystems, Thermo Fisher Scientific) according to the manufacturer's recommendation. For qRT-PCR, obtained cDNA was diluted 1:10 in nuclease-free water and master mixes were prepared with primer and iTaq SYBR green master mix (Biorad, Hercules, CA) or PowerUp SYBR green master mix (Thermo Fisher Scientific). Primers were obtained from a commercial source (Quantitect, Qiagen or Kicqstart, Sigma-Aldrich, St. Louis, MO) or designed and manufactured (Stanford University, see Table E1). QRT-PCR was run in 96 or 384 well plates in a CFX96 or CFX384 touch qRT-PCR system (Biorad) with the following program: initial step at 95˚C for 30 s. Then, 45 cycles with then following conditions: 95.0˚C for 5 s, followed by 60.0˚C for 30 s. After a final step of 95˚C for 10s, a melting curve was generated by increasing the temperature from 65.0 to 95.0˚C in 0.5˚C increments/5 s. The following primers were used for amplification: Quantitect (Qiagen): human *B2M* (Hs_B2M_1_SG), human *RRN18S* (18SRNA, Hs_RRN18S_1_SG), human *TLR3* (Hs_TLR3_1_SG), rat *Tlr3* (Rn_Tlr3_2_SG), human *CXCL10* (Hs_CXCL10_1_SG), rat *Cxcl10* (Rn_Cxcl10_1_SG). Kicqstart (Sigma-Aldrich): human *TBP* (forward: FH1_TBP and reverse: RH1_TBP), human *DDX58* (forward: FH1_DDX58

Copyright © 2018 by the American Thoracic Society

AJRCCM Articles in Press. Published on 13-September-2018 as 10.1164/rccm.201707-1370OC

and reverse: RH1_DDX58), human *IFIH1* (forward: FH1_IFIH1 and reverse: RH1_IFIH1), human *IL6* (forward: FH_IL6 and reverse: RH_IL6), human *IL10* (forward: FH2_IL10 and reverse: RH2_IL10), human *RPS20* (forward: FH1_RPS20 and reverse: RH1_RPS20), rat *Il10* (forward: FR1_Il10 and reverse: RR1_Il10), rat *Edn1* (forward: FR1_Edn1 and reverse: RR1_Edn1), rat *Gusb* (forward: FR1_Gusb and reverse: RR1_Gusb), rat *Tbp* (forward: FR1_Tbp and reverse: RR1_Tbp). For calculation of the results, the most stable housekeeping or the two most stable housekeeping genes were identified using the relative expression software tool (REST) from Pfaffl *et al.* (E10) from a set of genes that included *RRN18S*, *B2M*, *GUSB*, *TBP* and *RPS20*. If two housekeeping genes were used, the geometric mean of two housekeeping genes was used as reference. Analysis was performed according to the principles set forth by Pfaffl, M. (E11).

Flow cytometry

For surface marker expression of $CD117^+$ EC, cells were removed from culture vessel and suspended at a concentration of 10^6 cells/100 µl flow reaction buffer [2% fetal bovine serum (FBS)/PBS]. Then, primary labeled antibodies for CD45 and CD11b/c (both BD Biosciences) were added for 30 min at room temperature in the dark to detect CD11b/c and CD45. For vWF (Abcam), permeabilization using Cytofix/Cytoperm buffer and Permwash wash buffer (both BD Bioscience, San Jose, CA) was performed for 20 min. prior to antibody incubation according to the manufacturer's recommendations. The staining was analyzed on a BD FACS Canto machine and analysis was performed using FlowJo software (FlowJo, LLC, Ashland, OR).

For Annexin V binding assay, allophycocyanin (APC) Annexin V (BD Biosciences)

Copyright © 2018 by the American Thoracic Society

AJRCCM Articles in Press. Published on 13-September-2018 as 10.1164/rccm.201707-1370OC

was used according to the manufacturer's recommendations. 10^5 cells dissolved in 100 µl binding buffer were incubated for 15 min at room temperature (in the dark) with 3-5 µl of APC Annexin V and 5 µl of 7-Amino-Actinomycin (7-AAD), then diluted with 400 µl of binding buffer. The staining was analyzed on a BD FACS Canto machine within 1 hr and analysis was performed using FlowJo 10 software (FlowJo, LLC, Ashland, OR).

Lung cell single suspension and flow cytometry staining for inflammatory cells was performed as published previously (E1).

Protein isolation and Western blot

Whole cell protein lysate was prepared as published previously (E1; E7). For cell culture experiments, 10-20 µg protein and for whole lung tissue protein lysate, 50 µg protein was loaded onto Nu-PAGE 4-12% Bis-Tris protein gels and resolved by SDS-PAGE. Then, protein was blotted onto a nitrocellulose membrane for antibody staining and chemiluminiscence detection (Amersham ECL reagent, GE Healthcare Life Sciences, Marlborough, MA). The following antibodies were used for detection: TLR3 (LifeSpan Biosciences), TLR3 (abcam), p65 (Cell Signaling), c-Jun (Cell Signaling), Lamin B (Santa Cruz Biotechnology), IL-10 (R&D Systems) and as loading control, β-actin (Sigma). Images were obtained with a Chemidoc XRS+ gel imager with ImageLab software (Biorad, Hercules, CA), or developed with Blue Autoradiography films (GeneMate, VWR, Radnor, PA) and scanned with an Perfection V700 scanner (Epson, Long Beach, CA).

Copyright © 2018 by the American Thoracic Society

AJRCCM Articles in Press. Published on 13-September-2018 as 10.1164/rccm.201707-1370OC

Immunohistochemistry/immunofluorescence staining and morphometry

Immunohistochemistry (IHC) and double/triple Immunofluorescence (IF) stainings were performed according to established protocols as previously published (E1; E2; E7). The following primary antibodies were used: caveolin-1 (Cell Signaling Technologies, Danvers, MA), cleaved caspase-3 (Cell Signaling Technologies), proliferating cell nuclear antigen (PCNA, Cell Signaling Technologies), TLR3 (LifeSpan Biosciences), TLR3 (abcam), α-SMA (Sigma-Aldrich), vWF (DAKO cytomation). For Terminal deoxynucleotidyl transferase dUTP nick end labeling (TUNEL) and TLR3 double IF, lung tissue sections were stained using the ApopTag Fluorescein *In Situ* Apoptosis Detection Kit (Millipore Sigma, Burlington, MA) and TLR3 antibody (abcam) according to the manufacturer's recommendation similar to previously published protocols (E7; E12). To quantify IHC staining for cleaved caspase-3, PCNA and TLR3, the number of positive cells and total cells were enumerated in 10 randomly acquired pulmonary arteries per animal by a blinded investigator as previously described using the cell counter plugin for Fiji (E1; E2; E7). For analysis of cleaved caspase-3 in human lung tissue sections and TLR3 in rat lungs, cleaved caspase-3^+ or $TLR3^+$ endothelial/intima cells were counted and presented as fraction of total endothelial/intima cells. For analysis of cleaved caspase-3^+ IHC in the left ventricle (apoptotic index), 5 images of left ventricular tissue were randomly acquired at a magnification of 400x. Cleaved caspase-3^+ cells were counted and presented as fraction of total cells per field of view.

For analysis of left ventricular capillary density, 5 images of left ventricular tissue stained for caveolin-1 (IHC) were randomly acquired at a magnification of 400x. Caveolin-1^+ tissue area (=capillary area) was measured for each image using “color deconvolution”

Copyright © 2018 by the American Thoracic Society

AJRCCM Articles in Press. Published on 13-September-2018 as 10.1164/rccm.201707-1370OC

plugin using thresholding and area measurement in Fiji (E8), similar to previous published work (E7). To obtain capillary density, caveolin-1^{+} area was divided by the total tissue area. Objectivity in all analyses was further ensured by providing each animal with a numerical code to mask treatment groups.

For measurement of muscularization in pulmonary arteries, images of α-SMA IHC stained sections were randomly taken with an AXIO imager.A1 microscope, Axiocam HRc camera and Axiovision software (all Zeiss, Jena, Germany) at 100× magnification. Objectivity was ensured by providing each animal with a numerical code to mask treatment groups. Media thickness (MT) and external diameter (ED) were measured as published before and media wall thickness (MWT) was calculated according to the formula: MWT=[(2×MT)/ED]×100% (E7). For MWT in mice, MT was obtain in slides with IHC staining for α-SMA and was divided by the vessel area and provided as percent MWT. Pulmonary arteries were categorized as follows: small-sized 25 μm < ED < 50 m, medium-sized 50 μm ≤ ED < 100 μm. For each animal, 30-40 pulmonary arteries were measured in two orthogonal directions using Fiji image analysis software (E8). For analysis of chronic hypoxic PH in rats and chronic hypoxia/SU5416 in mice, the pulmonary arteries were further classified as ‘muscularized’, ‘partially muscularized’ and ‘non-muscularized’.

Vascular occlusion was quantified in sections stained for vWF IHC as published previously to obtain the fraction of small-sized pulmonary arteries that were classified as ‘patent’, ‘partially occluded’ and ‘completely obstructed’ (E1). Objectivity was here also ensured by providing each animal with a numerical code to mask treatment groups, random acquisition of images and blinded investigator.

Copyright © 2018 by the American Thoracic Society

AJRCCM Articles in Press. Published on 13-September-2018 as 10.1164/rccm.201707-1370OC

REFERENCES

E1. Farkas, D, Alhussaini, AA, Kraskauskas, D, Kraskauskiene, V, Cool, CD, Nicolls, MR, Natarajan, R, Farkas, L. Nuclear factor κB inhibition reduces lung vascular lumen obliteration in severe pulmonary hypertension in rats. Am J Respir Cell Mol Biol 2014; 51: 413-425.

E2. Farkas, D, Kraskauskas, D, Drake, JI, Alhussaini, AA, Kraskauskiene, V, Bogaard, HJ, Cool, CD, Voelkel, NF, Farkas, L. CXCR4 inhibition ameliorates severe obliterative pulmonary hypertension and accumulation of C-kit$^+$ cells in rats. PLoS One 2014; 9: e89810.

E3. Ciuclan, L, Bonneau, O, Hussey, M, Duggan, N, Holmes, AM, Good, R, Stringer, R, Jones, P, Morrell, NW, Jarai, G, Walker, C, Westwick, J, Thomas, M. A novel murine model of severe pulmonary arterial hypertension. Am J Respir Crit Care Med 2011; 184: 1171-1182.

E4. van Beijnum, JR, Rousch, M, Castermans, K, van der Linden, E, Griffioen, AW. Isolation of endothelial cells from fresh tissues. Nat Protoc 2008; 3: 1085-1091.

E5. Gong, H, Liu, M, Klomp, J, Merrill, BJ, Rehman, J, Malik, AB. Method for Dual Viral Vector Mediated CRISPR-Cas9 Gene Disruption in Primary Human Endothelial Cells. Sci Rep 2017; 7: 42127.

E6. Voets, O, Tielen, F, Elstak, E, Benschop, J, Grimbergen, M, Stallen, J, Janssen, R, van Marle, A, Essrich, C. Highly efficient gene inactivation by adenoviral CRISPR/Cas9 in human primary cells. PLOS ONE 2017; 12: e0182974.

Copyright © 2018 by the American Thoracic Society

AJRCCM Articles in Press. Published on 13-September-2018 as 10.1164/rccm.201707-1370OC

E7. Farkas, L, Farkas, D, Ask, K, Moller, A, Gauldie, J, Margetts, P, Inman, M, Kolb, M. VEGF ameliorates pulmonary hypertension through inhibition of endothelial apoptosis in experimental lung fibrosis in rats. J Clin Invest 2009; 119: 1298-1311.

E8. Schindelin, J, Arganda-Carreras, I, Frise, E, Kaynig, V, Longair, M, Pietzsch, T, Preibisch, S, Rueden, C, Saalfeld, S, Schmid, B, Tinevez, J-Y, White, DJ, Hartenstein, V, Eliceiri, K, Tomancak, P, Cardona, A. Fiji: an open-source platform for biological-image analysis. Nat Meth 2012; 9: 676-682.

E9. Yue, PY, Leung, EP, Mak, NK, Wong, RN. A simplified method for quantifying cell migration/wound healing in 96-well plates. J Biomol Screen 2010; 15: 427-433.

E10. Pfaffl, MW, Horgan, GW, Dempfle, L. Relative expression software tool (REST) for group-wise comparison and statistical analysis of relative expression results in real-time PCR. Nucleic Acids Res 2002; 30: e36.

E11. Pfaffl, MW. A new mathematical model for relative quantification in real-time RT-PCR. Nucleic Acids Res 2001; 29: e45.

E12. Farkas, L, Farkas, D, Gauldie, J, Warburton, D, Shi, W, Kolb, M. Transient overexpression of Gremlin results in epithelial activation and reversible fibrosis in rat lungs. Am J Respir Cell Mol Biol 2011; 44: 870-878.

Copyright © 2018 by the American Thoracic Society

AJRCCM Articles in Press. Published on 13-September-2018 as 10.1164/rccm.201707-1370OC

Supplemental Table

Gene name	direction	sequence
DDX58	forward	TACGCCTTCAGACATGGGAC
	reverse	TGGCTTGGGATGTGGTCTAC
IFIH1	forward	GGAGTCAAAGCCCACCATCT
	reverse	GTGAGCAACCAGGACGTAGG
IL10	forward	GACTTTAAGGGTTACCTGGGTTG
	reverse	TCACATGCGCCTTGATGTCTG
CXCL10	forward	GTGGCATTCAAGGAGTACCTC
	reverse	TGATGGCCTTCGATTCTGGATT
IL6	forward	TCCACAAGCGCCTTCGGTCC
	reverse	TGTCTGTGTGGGGCGGCTACA
RRN18S	forward	CGGCTACCACATCCAAGGAA
	reverse	GCTGGAATTACCGCCGCT

Supplemental Table E1. Designed primer sequences for human genes.

Copyright © 2018 by the American Thoracic Society

AJRCCM Articles in Press. Published on 13-September-2018 as 10.1164/rccm.201707-1370OC

SUPPLEMENTAL FIGURE LEGENDS

Figure E1. TLR3 deficiency is associated with endothelial apoptosis *in situ.* (**A**) Representative images (confocal microscopy) show strong endothelial TLR3 staining and no TUNEL$^+$ (apoptotic) cells in the intima of pulmonary arteries from control patient. Some TUNEL$^+$ cells are found in a perivascular infiltrate (asterisk). In contrast, PAH patients had reduced intimal TLR3 staining in remodeled pulmonary arteries and TUNEL$^+$ intima cells were found in areas with low cellular TLR3 expression (arrow). In the bottom row, small TUNEL$^+$ apoptotic bodies are found in the intima in a TLR3 deficient intima lesion area (arrows). The inserts show the indicated areas in more detail. Scale bars: 50 μm (overview on the left), 25 μm (higher detail images on the right). (**B**) Cleaved caspase-3$^+$ ECs were only very rarely detected in pulmonary arteries from control subjects, but pulmonary arteries from PAH patients contained cleaved caspase-3$^+$ intima cells (arrow: representative cleaved caspase-3$^+$ EC). The insert shows the area indicated by a dotted box in more detail. Scale bars: 50 μm (control), 100 μm (PAH). (**C**) Fraction of cleaved caspase-3$^+$ EC/intima cells in pulmonary arteries from control subjects and PAH patients. n=3 controls and 5 PAH patients (n=7-10 vessels for each patient). (**D**) Representative images for cleaved caspase-3 IHC shows more cleaved caspase-3$^+$ cells (mainly EC) in remodeled pulmonary arteries of TLR3$^{-/-}$ mice exposed to cHx/Su as compared with cHx/Su WT mice. (**E**) Quantification of % cleaved caspase-3$^+$ cells in WT and TLR3$^{-/-}$ mice exposed to cHx/Su (n=5 per group). Mean+SEM. **P*<0.05, ***P*<0.01 (C, E: t-test)

Copyright © 2018 by the American Thoracic Society

AJRCCM Articles in Press. Published on 13-September-2018 as 10.1164/rccm.201707-1370OC

Figure E2. Cleaved caspase$^+$ cells in pulmonary arteries of early cHx/Su rats and normoxic and chronic hypoxic TLR3 KO mice. (**A**) Representative images show presence of cleaved caspase-3$^+$ cells in the pulmonary artery wall of cHx/Su day 1 and 6 rats. Scale bar: 50 μm. (**B**) Quantification of the fraction of cleaved caspase-3$^+$ cells in the pulmonary arteries of naive, cHx/Su day 1 and cHx/Su day 6 rats. mean+SEM, n=3 per group. (One-way ANOVA)

Figure E3. Characterization of rat lung CD117$^+$ lin$^-$ CD31$^+$ EC (CD117$^+$ EC). CD117$^+$ EC form angiogenic tubes in matrigel (**A**) and are clonally expandable (**B**), suggesting a progenitor cell phenotype of these cells. Scale bars: 500 μm (matrigel), 100 μm (clonal assay). (**C**) The histograms show representative flow cytometry results indicating that CD117$^+$ EC express EC marker vWF, but lack expression of hematopoietic markers CD11b/c and CD45.

Figure E4. Loss of TLR3 expression is maintained in TLR3 CRISPR PAEC over passage. Representative images of immunocytochemistry demonstrate that most of the TLR3 CRISPR PAEC remain TLR3$^-$ after passage. Scale bar: 50 μm. Nuclear staining with DAPI.

Figure E5. Transfection vs. extracellular addition of Poly(I:C) in CD117$^+$ rat lung EC. Poly(I:C) transfection at a lower dose (2 μg/ml), which bypasses endosomal processing of dsRNA, increases mRNA expression of *Il10* (**A**), *Tlr3* (**B**) and *Cxcl10* (**C**) stronger than extracellular addition (25 μg/ml). mean+SEM; n=3 experiments/group. ** P<0.01, ***

Copyright © 2018 by the American Thoracic Society

AJRCCM Articles in Press. Published on 13-September-2018 as 10.1164/rccm.201707-1370OC

P<0.001 (One-way ANOVA).

Figure E6. Comparative gene expression following Poly(I:C) human lung microvascular EC (HLMVEC) and human umbilical vein EC (HUVEC). (**A-B**) Gene expression of *TLR3*, *DDX58* (RIG-I), *IFIH1* (MDA-5), *IL-6, CXCL10* and *IL10* in HLMVEC (A) and HUVEC (B) treated with 0.5 µg/ml Poly(I:C) and 50 µg/ml Poly(I:C) for 24h. There are substantial differences between the two types of EC: HUVEC have higher induction of *DDX58* and *IFIH1*, but fail to induce *CXCL10* and *IL10* compared to HLMVEC. mean+SEM. n=4-6 per group. **P*<0.05, ***P*<0.01, ****P*<0.001 (One-way ANOVA).

Figure E7. Comparison of Poly(I:C) effects on caspase 3/7 activity and reactive oxygen species (ROS) production. (**A**) Caspase 3/7 activity shows concentration-dependent increase in Poly(I:C)-treated HLMVEC under serum starvation (basal EGM). No increase in caspase 3/7 activity was found with Poly(I:C) stimulation in PAEC. n=4 (HLMVEC) and 6 (PAEC). (**B**) High dose of Poly(I:C) induced ROS production in HUVEC and PAEC. All bars mean+SEM. n=3 (HUVEC) and 6 (PAEC). ***P*<0.01, ****P*<0.001 (Two-way ANOVA).

Figure E8. Treatment of naive rats with high dose Poly(I:C) (10 mg/kg) or vehicle for 2 weeks with 3 doses/week. (**A**) Representative immunohistochemistry for vWF and α-SMA of naive rats treated with vehicle (veh) or Poly(I:C). Scale bars: 100 µm. (**B**) No change in RVSP in Poly(I:C) vs. vehicle. (**C**) Vehicle and Poly(I:C) treated rats exhibited

Copyright © 2018 by the American Thoracic Society

AJRCCM Articles in Press. Published on 13-September-2018 as 10.1164/rccm.201707-1370OC

no relevant degree of occlusion. Rarely, pulmonary arteries had vWF$^+$ cells in the lumen, causing classification as "partial" occlusion when the vWF$^+$ area exceeded 25% of the luminal area (see arrows in A). (**D**) Increased MWT in Poly(I:C)-treated naive rats. (**E**) More cleaved caspase-3$^+$ cells were found in the pulmonary artery wall of Poly(I:C) vs. vehicle-treated rats, whereas the fraction of PCNA$^+$ cells (**F**) only showed a trend towards higher proliferation rate. mean±SEM (scatter plot) and mean+SEM (bar graphs). n=3 per group. *P<0.05 (t-test).

Figure E9. Treatment with TLR3 agonist Poly(I:C) prevents chronic hypoxic PH. (**A**) Diagram of treatment protocol. (**B**) Poly(I:C) treatment prevented increase in RVSP [n=6 veh, n=4 Poly(I:C)]. (**C**) Representative images for α-SMA IHC show reduced thickness of the pulmonary artery smooth muscle layer in SD rats exposed to cHx after treatment with Poly(I:C) (10mg/kg, 3x/week). (**D**) Echocardiographically measured RV cardiac output. [n=6 veh, n=5 Poly(I:C)] (**E-F**) MWT (E) and fraction of small muscularized pulmonary arteries (25 μm<ED<50 μm) (F) were reduced after Poly(I:C) treatment in cHx rats (n=3 each). (**G-J**) Representative images (G, I) and quantification of fraction of cleaved caspase-3$^+$ (H) and PCNA$^+$ (J) cells (n=3 each) show reduced apoptosis and proliferation in the pulmonary arteries after Poly(I:C) treatment. All bars: mean+SEM, scatter plots: mean±SEM. *P<0.05 and ***P<0.0001, n.s.=not significant (t-test). Scale bars: 100 μm (C), 20 μm (G, I).

Figure E10. Preventive Poly(I:C) treatment does not change the fraction of inflammatory cells in the lungs of cHx/Su rats. In lung single cell suspensions, the

Copyright © 2018 by the American Thoracic Society

AJRCCM Articles in Press. Published on 13-September-2018 as 10.1164/rccm.201707-1370OC

fraction of $CD3^+$ (**A**), $CD4^+$ (**B**), $CD8^+$ (**C**), $CD45RA^+$ (**D**), $CD11b/c^+$ (**E**) and $granulocyte^+$ (**F**) cells was measured. Each bar: mean+SEM of n=3. (t-test)

Figure E11. Capillary density and apoptotic index in the left ventricles of chronic hypoxic rats after preventive treatment with vehicle or high-dose Poly(I:C) (day 21). The images show representative IHC for caveolin-1 (capillaries) and cleaved caspase-3 (apoptosis) of the left ventricle from cHx rats treated with vehicle (veh) or 10 mg/kg Poly(I:C) from day 1-21 (3x/week). The arrows indicate representative cleaved caspase-3^+ cells. Scale bars: 50 µm (caveolin-1), 25 µm (cleaved caspase-3). Each bar: mean+SEM of n=3. (t-test)

Figure E12. Capillary density and apoptotic index in the left ventricles of chronic hypoxia+SU5416 rats after therapeutic treatment with vehicle or high-dose Poly(I:C) (day 42). The images demonstrate representative IHC for caveolin-1 and cleaved caspase-3 of the left ventricle from cHx/Su rats treated with vehicle (veh) or 10 mg/kg Poly(I:C) from day 29-42 (3x/week). The arrows point to representative cleaved caspase-3^+ cells. Scale bars: 50 µm (caveolin-1), 25 µm (cleaved caspase-3). Each bar: mean+SEM of n=3. *P<0.05, **P<0.01 (t-test).

Copyright © 2018 by the American Thoracic Society

AJRCCM Articles in Press. Published on 13-September-2018 as 10.1164/rccm.201707-1370OC

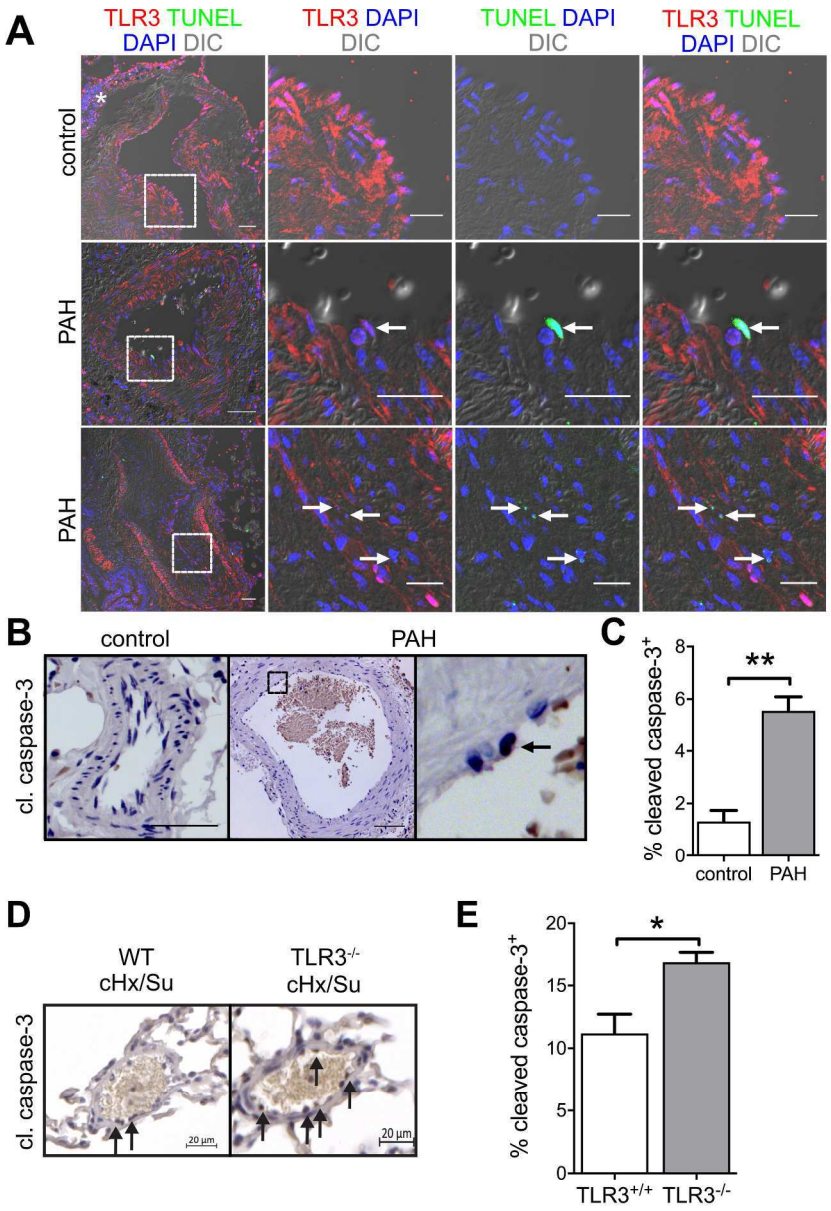

Figure E1. TLR3 deficiency is associated with endothelial apoptosis in situ. (**A**) Representative images (confocal microscopy) show strong endothelial TLR3 staining and no TUNEL$^+$ (apoptotic) cells in the intima of pulmonary arteries from control patient. Some TUNEL$^+$ cells are found in a perivascular infiltrate (asterisk). In contrast, PAH patients had reduced intimal TLR3 staining in remodeled pulmonary arteries and TUNEL$^+$ intima cells were found in areas with low cellular TLR3 expression (arrow). In the bottom row, small TUNEL$^+$ apoptotic bodies are found in the intima in a TLR3 deficient intima lesion area (arrows). The inserts show the indicated areas in more detail. Scale bars: 50 µm (overview on the left), 25 µm (higher detail images on the right). (**B**) Cleaved caspase-3$^+$ ECs were only very rarely detected in pulmonary arteries from control subjects, but pulmonary arteries from PAH patients contained cleaved caspase-3$^+$ intima cells (arrow: representative cleaved caspase-3$^+$ EC). The insert shows the area indicated by a dotted box in more detail. Scale bars: 50 µm (control), 100 µm (PAH). (**C**) Fraction of cleaved caspase-3$^+$ EC/intima cells in pulmonary arteries from control subjects and PAH patients. n=3 controls and 5 PAH patients (n=7-10 vessels for each patient). (**D**) Representative images for cleaved caspase-3 IHC shows more cleaved

Copyright © 2018 by the American Thoracic Society

AJRCCM Articles in Press. Published on 13-September-2018 as 10.1164/rccm.201707-1370OC

caspase-3^{+} cells (mainly EC) in remodeled pulmonary arteries of $TLR3^{-/-}$ mice exposed to cHx/Su as compared with cHx/Su WT mice. (**E**) Quantification of % cleaved caspase-3^{+} cells in WT and $TLR3^{-/-}$ mice exposed to cHx/Su (n=5 per group). Mean+SEM. *P<0.05, **P<0.01 (C, E: t-test)

212x296mm (300 x 300 DPI)

Copyright © 2018 by the American Thoracic Society

AJRCCM Articles in Press. Published on 13-September-2018 as 10.1164/rccm.201707-1370OC

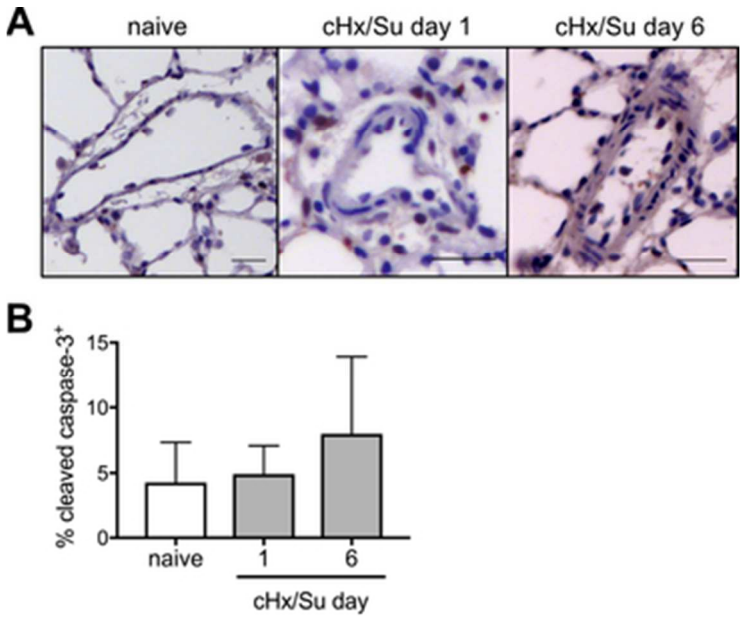

Figure E2. Cleaved caspase^{+} cells in pulmonary arteries of early cHx/Su rats and normoxic and chronic hypoxic TLR3 KO mice. (**A**) Representative images show presence of cleaved caspase-3+ cells in the pulmonary artery wall of cHx/Su day 1 and 6 rats. Scale bar: 50 µm. (**B**) Quantification of the fraction of cleaved caspase-3^{+} cells in the pulmonary arteries of naive, cHx/Su day 1 and cHx/Su day 6 rats. mean+SEM, n=3 per group. (One-way ANOVA)

30x25mm (300 x 300 DPI)

Copyright © 2018 by the American Thoracic Society

AJRCCM Articles in Press. Published on 13-September-2018 as 10.1164/rccm.201707-1370OC

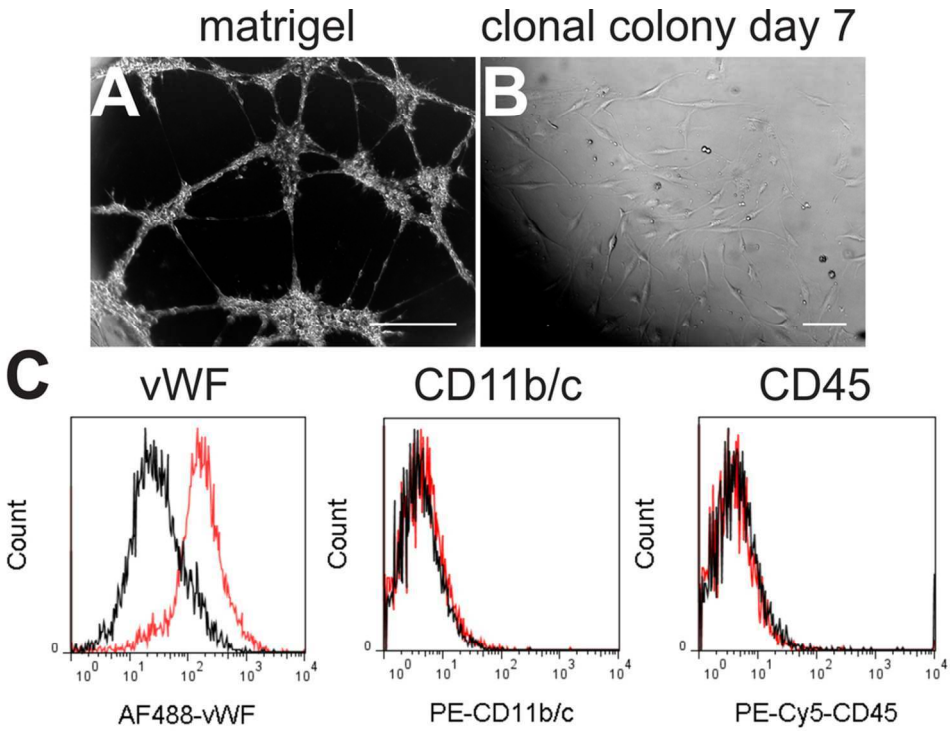

Figure E3. Characterization of rat lung CD117^{+} lin^{-} CD31^{+} EC (CD117^{+} EC). CD117+ EC form angiogenic tubes in matrigel (**A**) and are clonally expandable (**B**), suggesting a progenitor cell phenotype of these cells. Scale bars: 500 µm (matrigel), 100 µm (clonal assay). (**C**) The histograms show representative flow cytometry results indicating that CD117^{+} EC express EC marker vWF, but lack expression of hematopoietic markers CD11b/c and CD45.

94x69mm (300 x 300 DPI)

Copyright © 2018 by the American Thoracic Society

AJRCCM Articles in Press. Published on 13-September-2018 as 10.1164/rccm.201707-1370OC

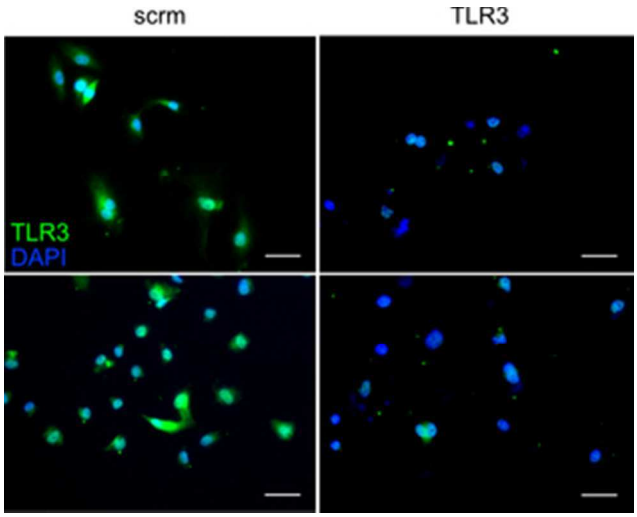

Figure E4. Loss of TLR3 expression is maintained in TLR3 CRISPR PAEC over passage.
Representative images of immunocytochemistry demonstrate that most of the TLR3 CRISPR PAEC remain TLR3$^-$ after passage. Scale bar: 50 μm. Nuclear staining with DAPI.

26x21mm (300 x 300 DPI)

Copyright © 2018 by the American Thoracic Society

AJRCCM Articles in Press. Published on 13-September-2018 as 10.1164/rccm.201707-1370OC

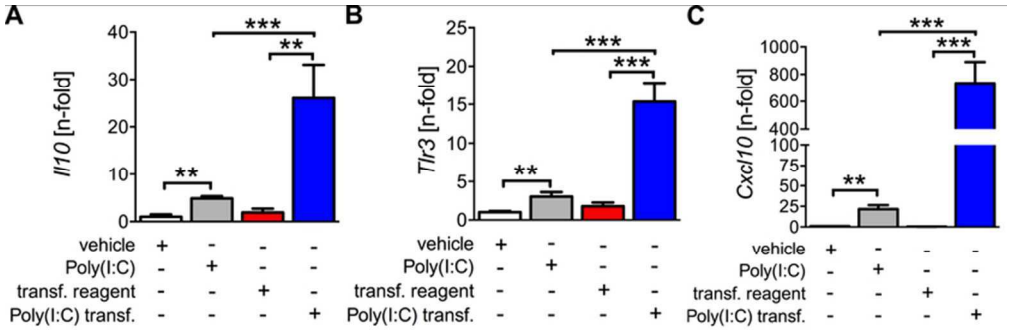

Figure E5. Transfection vs. extracellular addition of Poly(I:C) in CD117^{+} rat lung EC. Poly(I:C) transfection at a lower dose (2 µg/ml), which bypasses endosomal processing of dsRNA, increases mRNA expression of *Il10* (**A**), *Tlr3* (**B**) and *Cxcl10* (**C**) stronger than extracellular addition (25 µg/ml). mean+SEM; n=3 experiments/group. ***P*<0.01, ****P*<0.001 (One-way ANOVA).

35x11mm (600 x 600 DPI)

Copyright © 2018 by the American Thoracic Society

AJRCCM Articles in Press. Published on 13-September-2018 as 10.1164/rccm.201707-1370OC

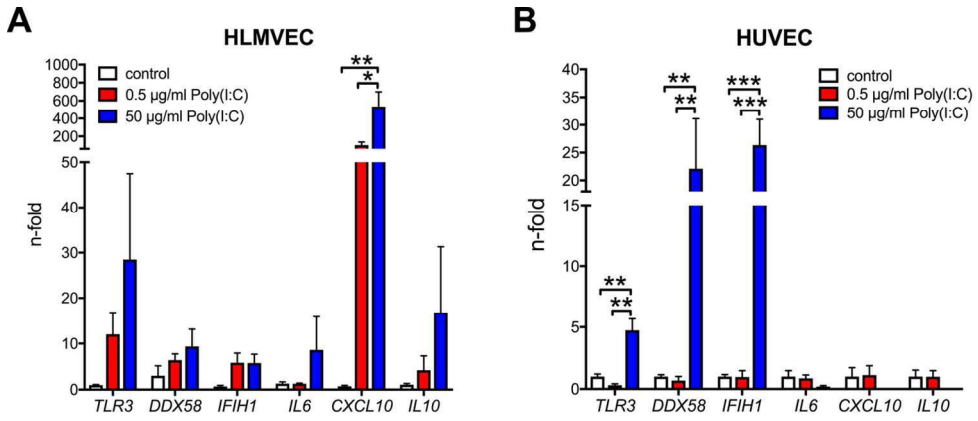

Figure E6. Comparative gene expression following Poly(I:C) human lung microvascular EC (HLMVEC) and human umbilical vein EC (HUVEC). (**A-B**) Gene expression of *TLR3*, *DDX58* (RIG-I), *IFIH1* (MDA-5), *IL6*, *CXCL10* and *IL10* in HLMVEC (A) and HUVEC (B) treated with 0.5 µg/ml Poly(I:C) and 50 µg/ml Poly(I:C) for 24h. There are substantial differences between the two types of EC: HUVEC have higher induction of *DDX58* and *IFIH1*, but fail to induce *CXCL10* and *IL10* compared to HLMVEC. mean+SEM. n=4-6 per group. **P*<0.05, ***P*<0.01, ****P*<0.001 (One-way ANOVA).

62x25mm (600 x 600 DPI)

Copyright © 2018 by the American Thoracic Society

AJRCCM Articles in Press. Published on 13-September-2018 as 10.1164/rccm.201707-1370OC

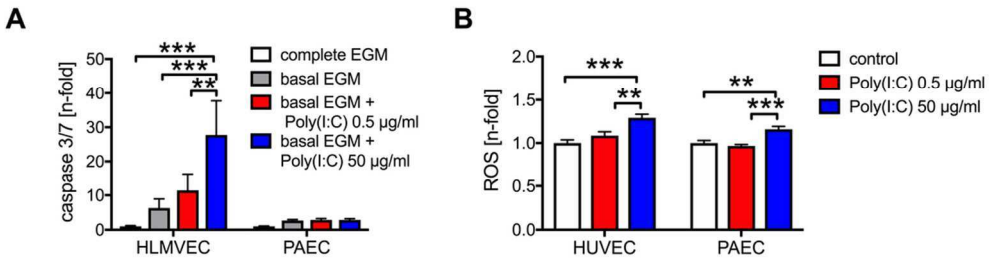

Figure E7. Comparison of Poly(I:C) effects on caspase 3/7 activity and reactive oxygen species (ROS) production. (**A**) Caspase 3/7 activity shows concentration-dependent increase in Poly(I:C)-treated HLMVEC under serum starvation (basal EGM). No increase in caspase 3/7 activity was found with Poly(I:C) stimulation in PAEC. n=4 (HLMVEC) and 6 (PAEC). (**B**) High dose of Poly(I:C) induced ROS production in HUVEC and PAEC. All bars mean+SEM. n=3 (HUVEC) and 6 (PAEC). ***P*<0.01, ****P*<0.001 (Two-way ANOVA).

49x13mm (600 x 600 DPI)

Copyright © 2018 by the American Thoracic Society

AJRCCM Articles in Press. Published on 13-September-2018 as 10.1164/rccm.201707-1370OC

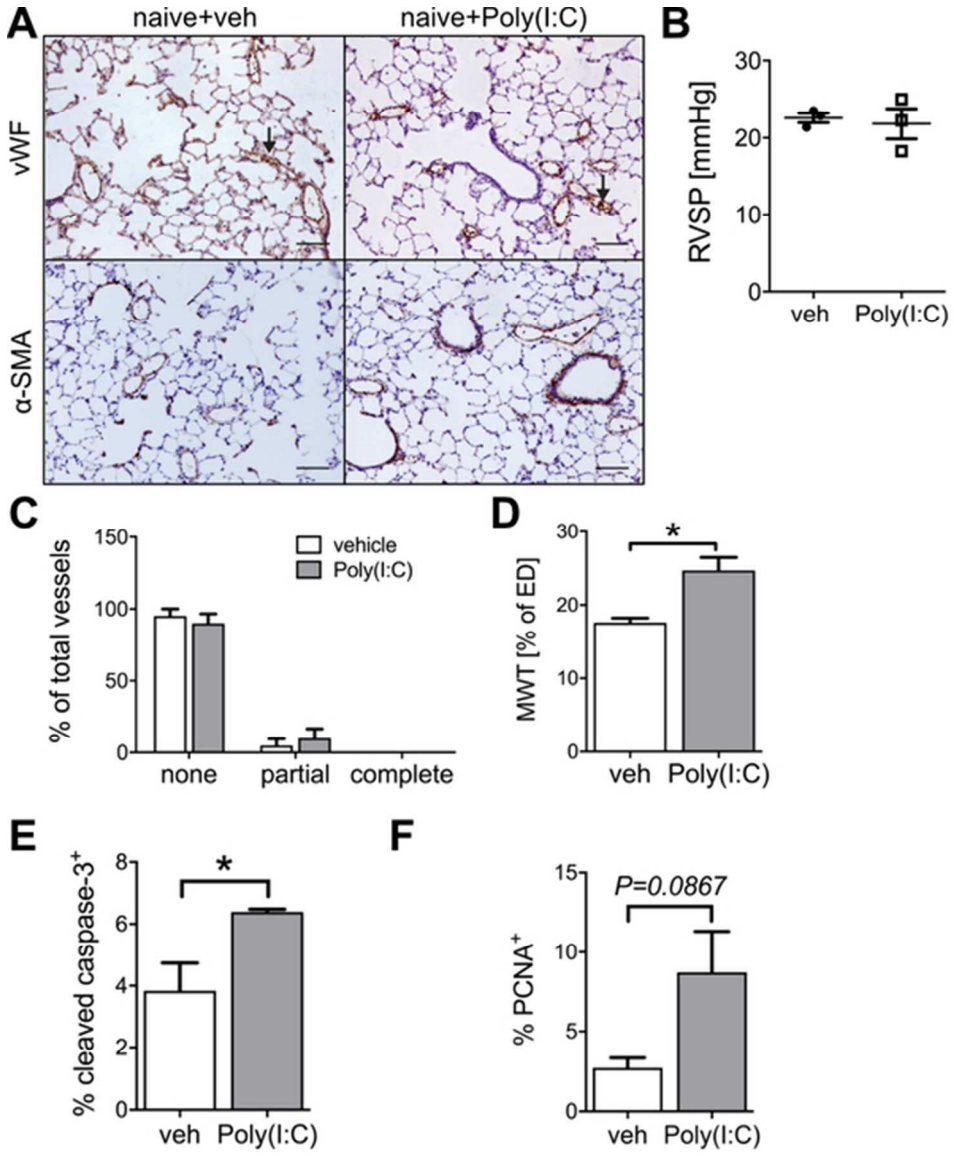

Figure E8. Treatment of naive rats with high dose Poly(I:C) (10 mg/kg) or vehicle for 2 weeks with 3 doses/week. (**A**) Representative immunohistochemistry for vWF and α-SMA of naive rats treated with vehicle (veh) or Poly(I:C). Scale bars: 100 μm. (**B**) No change in RVSP in Poly(I:C) vs. vehicle. (**C**) Vehicle and Poly(I:C) treated rats exhibited no relevant degree of occlusion. Rarely, pulmonary arteries had vWF$^+$ cells in the lumen, causing classification as "partial" occlusion when the vWF$^+$ area exceeded 25% of the luminal area (see arrows in A). (**D**) Increased MWT in Poly(I:C)-treated naive rats. (**E**) More cleaved caspase-3$^+$ cells were found in the pulmonary artery wall of Poly(I:C) vs. vehicle-treated rats, whereas the fraction of PCNA$^+$ cells (**F**) only showed a trend towards higher proliferation rate. mean±SEM (scatter plot) and mean+SEM (bar graphs). n=3 per group. *P<0.05 (t-test).

53x61mm (300 x 300 DPI)

Copyright © 2018 by the American Thoracic Society

AJRCCM Articles in Press. Published on 13-September-2018 as 10.1164/rccm.201707-1370OC

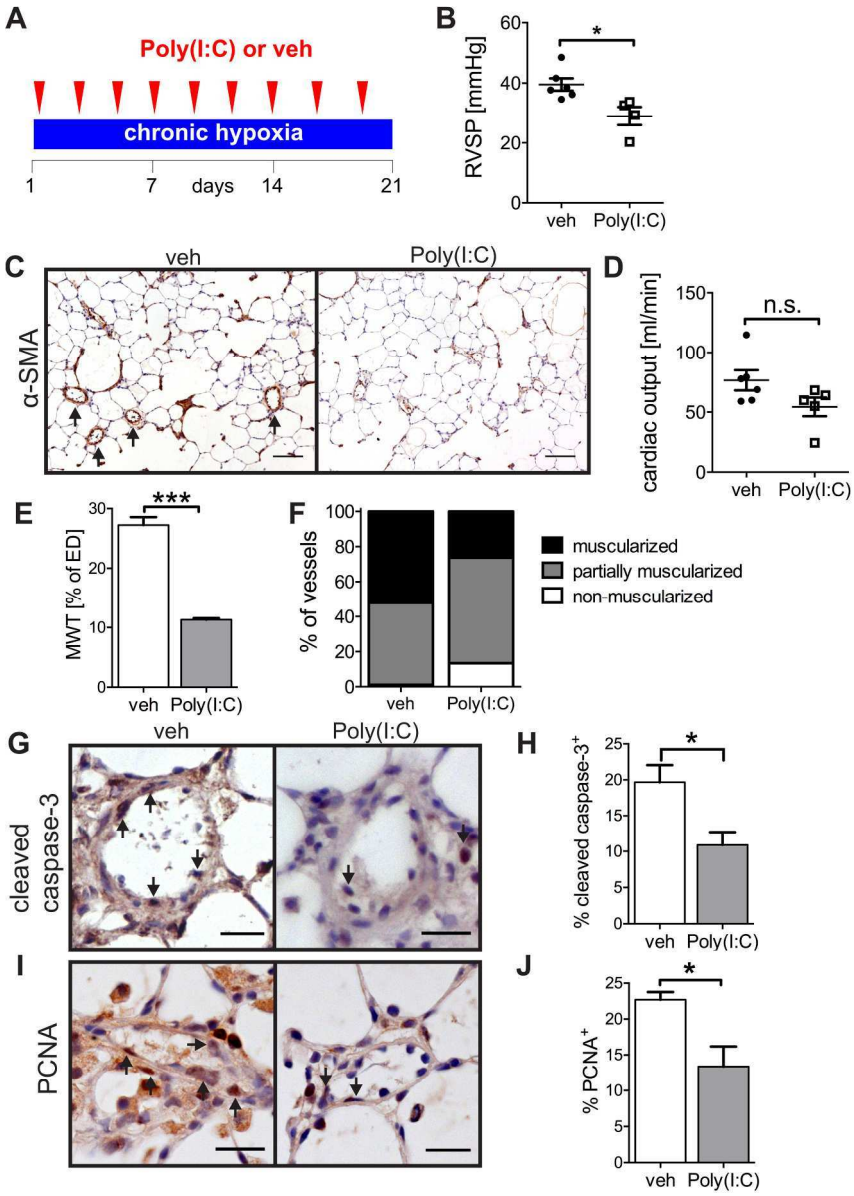

Figure E9. Treatment with TLR3 agonist Poly(I:C) prevents chronic hypoxic PH. (**A**) Diagram of treatment protocol. (**B**) Poly(I:C) treatment prevented increase in RVSP [n=6 veh, n=4 Poly(I:C)]. (**C**) Representative images for α-SMA IHC show reduced thickness of the pulmonary artery smooth muscle layer in SD rats exposed to cHx after treatment with Poly(I:C) (10mg/kg, 3x/week). (**D**) Echocardiographically measured RV cardiac output. [n=6 veh, n=5 Poly(I:C)] (**E-F**) MWT (E) and fraction of small muscularized pulmonary arteries (25 μm<ED<50 μm) (F) were reduced after Poly(I:C) treatment in cHx rats (n=3 each). (**G-J**) Representative images (G, I) and quantification of fraction of cleaved caspase-3$^+$ (H) and PCNA$^+$ (J) cells (n=3 each) show reduced apoptosis and proliferation in the pulmonary arteries after Poly(I:C) treatment. All bars: mean+SEM, scatter plots: mean±SEM. *P<0.05 and ***P<0.0001, n.s.=not significant (t-test). Scale bars: 100 μm (C), 20 μm (G, I).

212x291mm (300 x 300 DPI)

Copyright © 2018 by the American Thoracic Society

AJRCCM Articles in Press. Published on 13-September-2018 as 10.1164/rccm.201707-1370OC

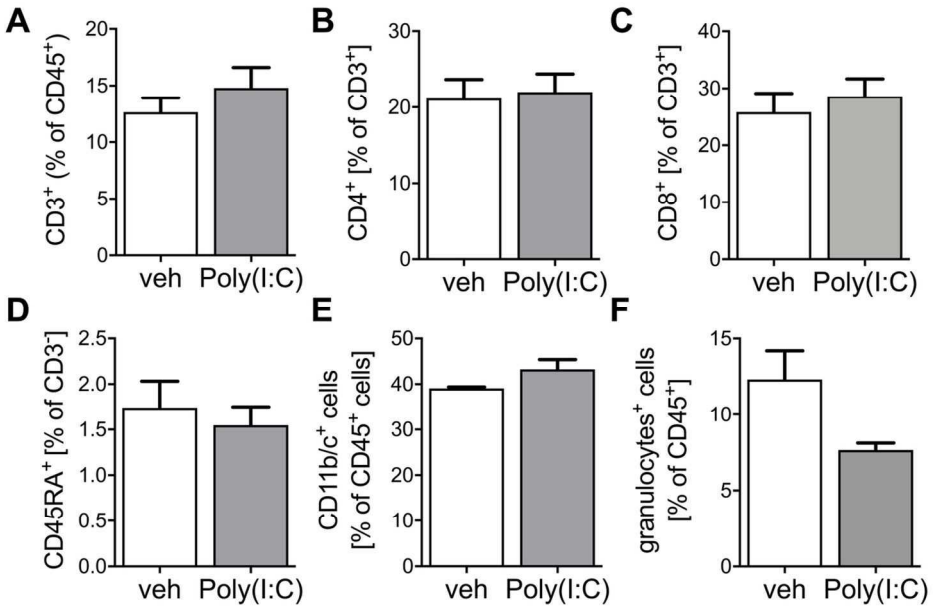

Figure E10. Preventive Poly(I:C) treatment does not change the fraction of inflammatory cells in the lungs of cHx/Su rats. In lung single cell suspensions, the fraction of $CD3^+$ (**A**), $CD4^+$ (**B**), $CD8^+$ (**C**), $CD45RA^+$ (**D**), $CD11b/c^+$ (**E**) and $granulocyte^+$ (**F**) cells was measured. Each bar: mean+SEM of n=3. (t-test)

59x37mm (600 x 600 DPI)

Copyright © 2018 by the American Thoracic Society

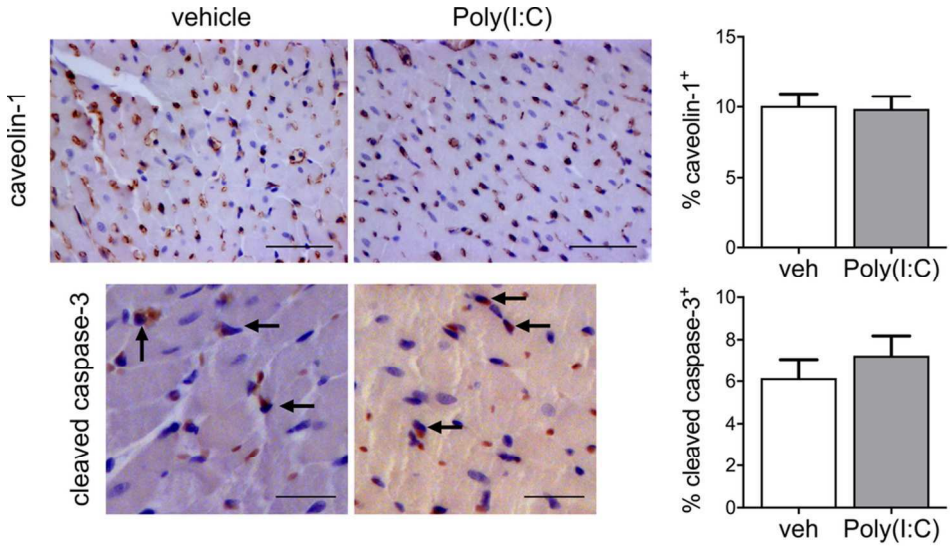

Figure E11. Capillary density and apoptotic index in the left ventricles of chronic hypoxic rats after preventive treatment with vehicle or high-dose Poly(I:C) (day 21). The images show representative IHC for caveolin-1 (capillaries) and cleaved caspase-3 (apoptosis) of the left ventricle from cHx rats treated with vehicle (veh) or 10 mg/kg Poly(I:C) from day 1-21 (3x/week). The arrows indicate representative cleaved caspase-3$^+$ cells. Scale bars: 50 µm (caveolin-1), 25 µm (cleaved caspase-3). Each bar: mean+SEM of n=3. (t-test)

95x51mm (300 x 300 DPI)

Copyright © 2018 by the American Thoracic Society

AJRCCM Articles in Press. Published on 13-September-2018 as 10.1164/rccm.201707-1370OC

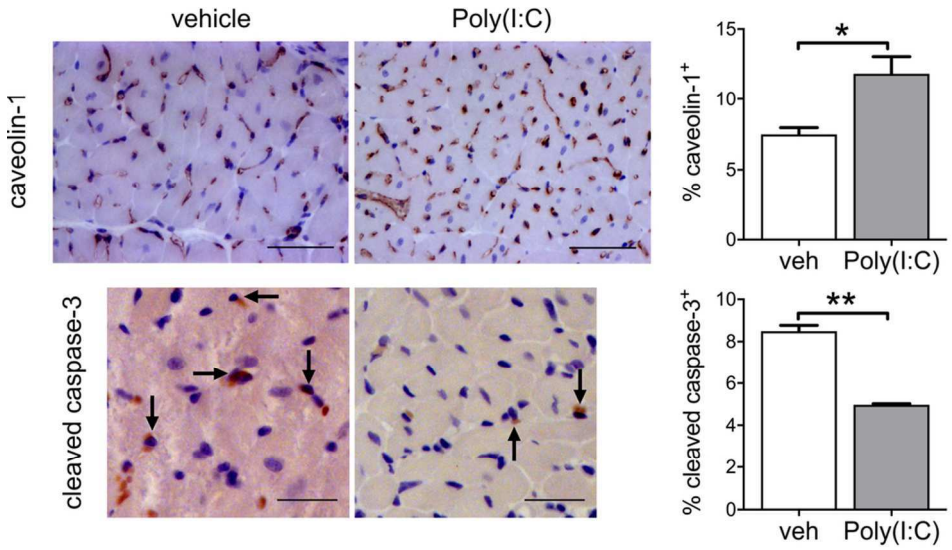

Figure E12. Capillary density and apoptotic index in the left ventricles of chronic hypoxia+SU5416 rats after therapeutic treatment with vehicle or high-dose Poly(I:C) (day 42). The images demonstrate representative IHC for caveolin-1 and cleaved caspase-3 of the left ventricle from cHx/Su rats treated with vehicle (veh) or 10 mg/kg Poly(I:C) from day 29-42 (3x/week). The arrows point to representative cleaved caspase-3^+ cells. Scale bars: 50 µm (caveolin-1), 25 µm (cleaved caspase-3). Each bar: mean+SEM of n=3. *P<0.05, **P<0.01 (t-test).

96x51mm (300 x 300 DPI)

Copyright © 2018 by the American Thoracic Society